Journal Pre-proof

Chitosan/γ-PGA nanoparticles-based immunotherapy as adjuvant to radiotherapy in breast cancer

Flávia Castro, Marta L. Pinto, Catarina L. Pereira, Karine Serre, Mário A. Barbosa, Karim Vermaelen, Fátima Gärtner, Raquel M. Gonçalves, Olivier de Wever, Maria J. Oliveira

PII: S0142-9612(20)30464-6

DOI: https://doi.org/10.1016/j.biomaterials.2020.120218

Reference: JBMT 120218

To appear in: *Biomaterials*

Received Date: 8 April 2020

Revised Date: 5 June 2020

Accepted Date: 22 June 2020

Please cite this article as: Castro Flá, Pinto ML, Pereira CL, Serre K, Barbosa MáA, Vermaelen K, Gärtner Fá, Gonçalves RM, de Wever O, Oliveira MJ, Chitosan/γ-PGA nanoparticles-based immunotherapy as adjuvant to radiotherapy in breast cancer, *Biomaterials* (2020), doi: https://doi.org/10.1016/j.biomaterials.2020.120218.

Chitosan/γ-PGA nanoparticles-based immunotherapy as adjuvant to radiotherapy in breast cancer

Flávia Castro[a,b,c], Marta L. Pinto[a,b,d#], Catarina L. Pereira[a,b#], Karine Serre[e], Mário A. Barbosa[a,b,c], Karim Vermaelen[f,g], Fátima Gärtner[a,c,h], Raquel M. Gonçalves[a,b]*, Olivier de Wever[g,i]*, Maria J. Oliveira[a,b]*

[a] i3S - Instituto de Investigação e Inovação em Saúde, Universidade do Porto, Porto, Portugal,
[b] INEB - Instituto de Engenharia Biomédica, Universidade do Porto, Porto, Portugal,
[c] ICBAS - Instituto de Ciências Biomédicas Abel Salazar, Universidade do Porto, Porto, Portugal,
[d] CNC - Centro de Neurociências e Biologia Celular, Universidade de Coimbra, Coimbra, Portugal,
[e] IMM - Instituto de Medicina Molecular João Lobo Antunes, Faculdade de Medicina, Universidade de Lisboa, Lisboa, Portugal,
[f] Tumor Immunology Laboratory, Department of Pulmonary Medicine and Immuno-Oncology Network Ghent, Ghent University Hospital, Ghent, Belgium,
[g] CRIG - Cancer Research Institute Ghent, Ghent University, Belgium,
[h] IPATIMUP - Instituto de Patologia e Imunologia Molecular da Universidade do Porto, Porto, Portugal,
[i] LECR - Laboratory Experimental Cancer Research, Department of Radiation Oncology and Experimental Cancer Research, Ghent University, Belgium.

[#] equally contributing second authors
* equally contributing last authors

Corresponding author:

Maria José Oliveira, PhD

Tumor Microenvironment Interactions Group Leader
INEB - Instituto de Engenharia Biomédica
i3S - Instituto de Investigação e Inovação em Saúde, Universidade do Porto
Rua Alfredo Allen, 208 | 4200-135 Porto, Portugal
Telf: +351 220 408 800 | email: mariajo@ineb.up.pt

Abstract

Radiotherapy (RT) is an essential treatment modality for several types of cancer. Despite its therapeutic potential, RT is frequently insufficient to overcome the immunosuppressive nature of the tumor microenvironment, failing to control tumor metastases. Innovative immunomodulatory strategies, like immunostimulatory biomaterials could be used to boost the immunogenic effects of RT. Herein, we addressed the synergistic potential of immunostimulatory chitosan/poly(γ-glutamic acid) nanoparticles (Ch/γ-PGA NPs) combined with RT to induce antitumor immunity in the 4T1 orthotopic breast tumor mouse model. Non-treated animals had progressive primary tumor growth and developed splenomegaly and lung metastases. While RT decreased primary tumor burden, Ch/γ-PGA NPs-treatment decreased systemic immunosuppression and lung metastases. The combination therapy (RT+ Ch/γ-PGA NPs) synergistically impaired 4T1 tumor progression, which was associated with a significant primary tumor growth and splenomegaly reduction, a decrease in the percentage of splenic immunosuppressive myeloid cells and an increase in antitumoral $CD4^{+}IFN\text{-}\gamma^{+}$ population. Notably, animals from the combination therapy presented less and smaller lung metastatic foci and lower levels of the systemic pro-tumoral cytokines IL-3, IL-4, IL-10, and of the CCL4 chemokine, in comparison to non-treated animals. Overall, these results evidenced that Ch/γ-PGA NPs potentiate and synergize with RT, headlining their promising role as adjuvant anticancer strategies.

Keywords: nanoparticles, radiotherapy, immunomodulation, breast cancer, combination therapy, immunotherapy

Graphical Abstract

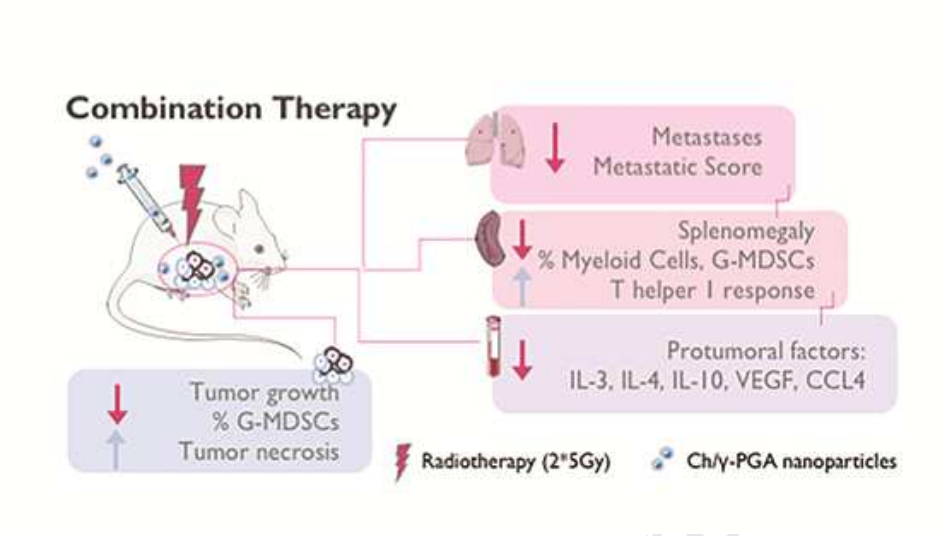

1. INTRODUCTION

Radiotherapy is an effective and broadly used treatment for several solid cancers, including breast, prostate, cervical, head and neck cancers [1]. Its biological principle is based on the induction of DNA double-strand breaks on aberrant proliferative and DNA-repair-deficient cells. Consequently, immunogenic cell death releases tumor-associated antigens into the tumor microenvironment as well as several damage-associated molecular patterns, eliciting an antitumor immune response [2, 3]. Nevertheless, tumor irradiation induces a wound healing response characterized by inflammation, extracellular matrix remodeling and infiltration of immunosuppressive myeloid cells, which may in turn facilitate therapeutic resistance and tumor relapse. This abundant myeloid immune infiltrate at the irradiated tumors essentially consists of tumor-associated macrophages (TAMs) and myeloid-derived suppressor cells (MDSCs), likely recruited to limit radiotherapy-induced tissue damage, contributing to dampen the antitumor immunity and potentiating the escape from immunosurveillance [4-6]. Accordingly, the accumulation of myeloid cells, including MDSCs and TAMs, has been associated with tumor progression and metastasis [7-10]. Importantly, the blockade of TAMs recruitment has been associated with better responses to immunotherapy in distinct preclinical studies [11], but no significant clinical benefits were observed yet [12]. Most recently, Kumar and co-workers demonstrated the importance of combining CSF1R blockade with CXCR2 inhibitors [13]. Given the functional plasticity of TAMs and granulocytic cells and their differential impact on tumor progression, the reprogramming of these cells, rather than their depletion, appears as a more effective therapeutic strategy [14, 15] to potentiate radiotherapy effects.

Our team has previously explored the effect of clinically relevant ionizing radiation doses (5*2Gy) on human macrophage function and on macrophage-cancer cell crosstalk. Accordingly, we demonstrated that besides the induced DNA damage, irradiated macrophages remained viable and metabolically active. Additionally, ionizing radiation drove macrophages towards a more pro-inflammatory like-profile, still preserving their ability to stimulate cancer cell invasion and angiogenesis [16]. Considering the infiltration of myeloid cells in the irradiated site, we propose targeting these cells following radiotherapy treatment in order to promote T cell-mediated antitumor immune response.

Biomaterials have been widely studied for vaccine delivery, since they could protect antigen and adjuvant molecules from degradation, increase lymphoid organ accumulation, and modulate antigen-presenting cell (APCs) functions. Several biomaterial-assisted cancer vaccines have shown great potential in preclinical and clinical development [17-22]. For example, synthetic high-density lipoprotein (sHDL) nanodiscs efficiently co-deliver tumor antigens and the adjuvant CpG to draining lymph nodes. These nanodiscs promoted dendritic cells (DCs) maturation and elicited cytotoxic T lymphocyte (CTL) responses. Additionally, their combination with immune checkpoint inhibitors further amplified the effect of nanodiscs vaccination, leading to the elimination of established tumors [18]. Others showed that nanodiscs combined with multiple TLR agonists are strong adjuvants for vaccines [23]. We recently reported that chitosan (Ch)/poly(γ-glutamic acid) (γ-PGA) nanoparticles (NPs) modulate immature DCs towards an immunostimulatory profile, eliciting CD4 T cell response. Furthermore, Ch/γ-PGA NPs reprogrammed IL-10-stimulated macrophages, characterized by an immunosuppressive phenotype, towards an immunostimulatory one, potentiating CD8 T cell response. Notably, Ch/γ-PGA NPs hindered the ability of macrophages and DCs to induce cancer cell invasion *in vitro* [24]. Therefore, the intrinsic immunostimulatory properties of Ch/γ-PGA NPs makes them good candidates for being used as adjuvants in cancer therapeutic immunomodulatory strategies.

Thus, the present work aims to evaluate *in vivo* the ability of Ch/γ-PGA NPs to synergize with radiotherapy to improve its antitumor effect by: (1) controlling primary tumor growth, (2) inhibiting lung metastasis, and (3) enhancing the immune response. In agreement, this report highlights the potential of Ch/γ-PGA NPs to be combined with radiotherapy as an anticancer therapeutic strategy, based on its immunostimulatory properties, and ability to better control breast cancer progression.

2. MATERIAL AND METHODS

2.1. Ch/γ-PGA NPs preparation and characterization

Ch/γ-PGA NPs were prepared as previously described [24]. Briefly, purified Ch (France-Chitine) with the degree of acetylation (DA) of 10.4 ± 1.6%, determined by Fourier transform infrared

spectroscopy using KBr pellets (FTIR-KBr), and molecular weight (MW) of 324 ± 27 kDa, determined by size-exclusion chromatography, was used. γ-PGA, with MW of 10-50 kDa and a purity level of 99.5%, was produced from *Bacillus subtilis* cultures, as described by Pereira *et al* [25]. Ch/γ-PGA NPs were prepared at a molar ratio of 1:1.5 (mol Ch:mol γ-PGA) by a co-acervation method. γ-PGA solution (0.2 mg/mL in 0.05 M Tris-HCl with 0.15 M NaCl buffer solution) was dropped to a Ch solution (0.2 mg/mL in 0.2 M AcOH), using a 1 mL syringe copulated to a syringe pump (KD Scientific Inc., Holliston, MA), at constant speed (3.6 µL/s), under high stirring conditions and at room temperature (RT). All solutions were prepared in buffer solution with pH adjusted to 5.0. After initial preparation, Ch/γ-PGA NPs were concentrated 10 times by centrifugation (13000 rpm, 30 minutes (min), 4 ºC). Ch/γ-PGA NPs size, polydispersion index and zeta potential were then evaluated by dynamic light scattering (DLS) in a ZetaSizer Nano Zs (Malvern Instruments), equipped with a He-Ne laser (λ=633 nm) and through NanoSight LM10-HS microscope (NanoSight, Amesbury, UK). Each NPs batch produced was tested and 3 measurements per sample were acquired. The stability of the Ch/γ-PGA NPs was previously studied by our group [25-28], being the electrostatic interactions between Ch and γ-PGA disrupted at physiological pH.

2.2. Cell lines

The 4T1 cell line expressing luciferase (4T1-Luc), a mouse triple negative breast cancer cell line, was obtained from Sibtech (Brookfield, CT, USA). Tumor cells were maintained/expanded in Dulbecco's Modified Eagle's Medium (Gibco; Life Technologies), supplemented with 10% (v/v) fetal calf serum (FCS) (Gibco; Life Technologies) and 1% (v/v) penicillin/streptomycin (Sigma) (cDMEM) at 37°C and 5% CO_2 humidified atmosphere. All cultures were regularly tested for Mycoplasma by using MycoAlert Plus Kit (Lonza, Basel, Switzerland).

2.5. Ethics Statement

All animal experiments were performed in strict accordance with the recommendations of the European Union Directive 2010/63/EU and the Helsinki declaration, following a protocol previously approved by the UZ-Ghent University Hospital Ethics Committee (ECD 17/124). At

the defined endpoints, mice were euthanized by cervical dislocation by trained personal, certified by the Portuguese Direção-Geral de Alimentação e Veterinária, to minimize suffering.

2.4. Animal studies

Four-week-old immunocompetent BALB/cByJ females (Charles River Laboratories, l' Arbresle Cedex, France) were injected orthotopically in the mammary fat pad with $1x10^6$ 4T1-luciferase cells, resuspended in 100 µl serum-free DMEM in Matrigel matrix (1:1) (Corning). Tumor implantation was confirmed by bioluminescence imaging after 24 hours of tumor cell injection. Mice were intraperitoneally injected with 150 mg/kg body weight D-luciferin (Caliper Life Sciences), 20 minutes before bioluminescence imaging, which was carried out by using an IVIS Lumina II (Caliper Life Sciences). Bioluminescent imaging was initiated by a cooled CCD camera in the IVIS with a 15-cm field of view, binning factor of 8, 1/f stop and open filter. Exposure times were set automatically, according to the luciferase signaling activity. Regions of interest (ROIs) were drawn for primary tumor and metastatic sites and were calculated through the IVIS software, expressed in total flux (photon/s).

After seven days of tumor cell inoculation, when tumors reached around 123 ± 12 mm^3, animals from radiotherapy (RT) and combinatory therapy (RT plus Ch/γ-PGA NPs) groups were locally irradiated with hypofractionated 10 Gy (2x5 Gy) using a Small Animal Radiation Research Platform, SARRP system (X-ray tube: ISOVOLT 225M2 X-ray source; SARRP system, XStrahl®, Surrey, UK), at a constant rate of 2.83 Gy/min, for 106 seconds. Ionizing radiation experiments were performed at days 7 and 10. The voltage of the X-ray source was fixed at 220 kV with a tube current of 13 mA, emitted from the 2.5 mm focal spot and filtered by a copper filter of 0.15 mm and a 5 mm x 5 mm collimator. After 3 days, animals from Ch/γ-PGA NPs and RT plus Ch/γ-PGA NPs groups were subcutaneously injected at the tumor site, 6 times along 2 weeks (d13, d16, d19, d22, d25 and d28) with Ch/γ-PGA NPs (0.7 mg/mL). The total dosage of Ch/γ-PGA NPs was 0.42 mg per mouse (22.1 mg Ch/γ-PGA NPs/kg mice). Tumor volume was measured using a caliper and calculated as (length × width × width)/2 (mm^3) and was normalized considering its volume prior any treatment. Tumor progression was followed by bioluminescence imaging every week. Animals were sacrificed at day 28.

2.5. Tumor and spleen digestion and stimulation

Primary tumors were collected 4 weeks after tumor cell inoculation, cut into small fragments and incubated with incomplete RPMI plus collagenase I (0.4 mg/mL), collagenase IV (1 mg/mL) and DNase (10 µg/mL) for 30 min at 37ºC. Spleens were collected and mechanically digested. Erythrocytes were lysed with red blood cell lysis buffer (Biolegend) for 3 minutes at room temperature. For lymphoid cell immunophenotyping, splenocytes were stimulated with Phorbol 12-myristate (PMA) (200 ng/mL, Sigma), ionomycin (1 µg/mL, Sigma) and Brefeldin A (BFA) (10 µg/mL, Sigma), for 4 hours at 37 °C.

2.6. Flow Cytometry

After stimulation, cells were washed in FACS buffer (PBS, 2% FBS, 0.01% sodium azide) and pre-treated with Fc blocking agent (anti-mouse CD16/CD32, Biolegend) for 10 minutes, to minimize non-specific antibody binding. Then, cells were stained in the dark, for 45 minutes at 4 ºC, with the following antibodies: CD3-PerCPcy5.5 (clone145-2C11, eBioscience), CD4-BV421 (clone RM4-5, Ebioscience), CD8 (clone 53-6.7, Biolegend), CD11b-Alexa 700 (clone M1/70, Biolegend), CD11c-FITC (clone N418, Biolegend), CD45-BV510 (clone 30-F11, Biolegend), CD45-APC (clone 30-F11, Biolegend), CD206-PerCPcy5.5 (clone C068C2, Biolegend), Ly6C-BV605 (clone HK1.4, Biolegend), Ly6G-BV421 (clone 1A8, Biolegend), F4/80-PEcy7 (clone BM8, Ebioscience) and MHC II-APCcy7 (clone M5/114.15.2, Ebioscience). The Aqua Zombie-BV510 and Live Dead-APC-Cy7 were used to confirm cell viability. After staining, cells were washed and fixed with 2% paraformaldehyde overnight. Cells were permeabilized with Permeabilization buffer (Invitrogen), in the dark, for 20 minutes at room temperature and stained for intracellular antigens, for 30 minutes at room temperature, using the following antibodies: IL-17-FITC (clone TC11-18H10, Biolegend), IFN-γ-BV605 (clone XMg1.2, Biolegend), TNF-α-PE (clone MP6-XT22, Ebioscience) and FoxP3-APC (clone FJK-16S, Ebioscience). Isotype-matched antibodies were used as negative controls. After additional washes, cells were acquired on a BD LSR Fortessa Flow Cytometer (BD Biosciences) and BD FACSDiva software. Results were analyzed using FlowJo software version 10 (TreeStar, Inc.).

2.7. Serum collection and analysis

Blood was collected from all animals by cardiac puncture to non-coated eppendorfs. Then, blood samples were centrifuged at 2500 rpm, for 30 minutes at room temperature and the serum fraction

was further centrifuged at 1200 rpm, 5 minutes, at 4 ºC to remove erythrocytes and stored at -80 ºC until further use. Samples were then analyzed for cytokines and chemokines using a mouse cytokine/chemokine array 31-multiplex (MD31) commercially available from Eve Technologies.

2.8. Histology

Mice breast primary tumors, lungs, liver, spleen and left kidney were fixed for 24-48 hours in formalin at room temperature. Afterwards, these organs were embedded in paraffin, sectioned into 3 µm thickness sections, and stained with hematoxylin and eosin. The metastatic score was made by three independent observers along the middle plan of the distinct lung lobules. Such score considered the presence or absence of metastatic foci and their size as: absence of foci (score I), small foci (score II), intermediate foci areas (score III) and large metastasized areas (score IV).

2.9. Statistical analysis

All graphs and statistical analysis were performed using GraphPad Prism Software version 7 (GraphPad-v7). The nonparametric unpaired Kruskal Wallis test was used for non-paired comparisons of more than two groups. The nonparametric Mann-Whitney test was used for comparisons between two independent groups. Statistical significance was considered when *p<0.05, **p<0.01, ***p<0.001.

3. RESULTS

3.1. Ch/γ-PGA NPs characterization

We have previously developed Ch/γ-PGA NPs and confirmed their capacity to reprogram immature DCs and anti-inflammatory macrophages into pro-inflammatory cells with the ability to promote T cell proliferation and impair cancer cell invasion [24]. Recent *in vivo* studies showed

no toxicity signs in inflammatory intervertebral disc rat model upon Ch/γ-PGA NPs treatment [29].

Here, we investigated the *in vivo* potential of these Ch/γ-PGA NPs as adjuvants to radiotherapy. Ch/γ-PGA NPs were prepared by dropping a γ-PGA solution to a Ch solution, under stirring at pH 5 at constant rate, as previously described (Fig. S1A) [24]. The molar ratio, polymer concentration, pH of interaction and stability were firstly optimized to prepare a low polydisperse solution with nano-sized stable Ch/γ-PGA particles [25]. Particles concentration, size, polydispersion index and zeta potential were evaluated by Dynamic light scattering (DLS) and NanoSight (Fig. S1B,C). The results indicated that Ch/γ-PGA NPs presented a constant size (210.8 ± 1.4 nm) with a reduced polydispersion index (0.20 ± 0.05), a positive zeta potential (18.7 ± 0.9 mV) and a spherical shape (Fig. S1D). Furthermore, the chemical composition of Ch/γ-PGA NPs was analyzed by FTIR. The spectrum of the Ch/γ-PGA NPs was compared with the spectra of both polymers alone [30]. In this spectrum, it is clear the characteristic saccharide peaks of Ch (in the 960−1180 cm^{-1} region), the C=O stretching vibrations of secondary amides in the solid form and of saturated aliphatic carboxylic acid dimers like γ-PGA (amide I band, adsorption at 1630−1680 cm−1), the N−H scissoring deformation peak at 1565 cm^{-1}, indicative of the presence of saturated primary amine groups, and also the N−H deformation and C−N stretching of secondary amides solids, which include the amide II band of γ-PGA. The peak indicative of the C−O stretching of carboxylic acid dimers (1320−1210 cm^{-1} region), present in γ-PGA spectrum [30] appears to be low in Ch/γ-PGA NPs spectrum. These results suggest the presence of both polymers, Ch and γ-PGA, in the formulation of Ch/γ-PGA NPs.

3.2. Single and combination therapies do not affect mice body weight nor liver and kidney histology

The murine mammary 4T1 model is well described in the literature [31] and its poor immunogenicity and spontaneous metastasis formation in syngeneic mice make it an attractive were preclinical model to evaluate new anticancer therapies. Thus, luciferase-expressing 4T1 cells injected in the mammary fat pad of 4 weeks old BALB/cByJ mice. At the seventh and tenth day after tumor inoculation, animals from RT and RT+Ch/γ-PGA NPs (RT+NPs) groups were locally irradiated with 10 Gy, using a fractionated scheme (2*5 Gy). After 3 days, animals from

RT+NPs or NPs group were boosted with local subcutaneous Ch/γ-PGA NPs injections, three times/week, for two weeks (Fig. 1A). Animal body weight was monitored weekly, and no alteration was observed in any condition (Fig. S2A). At day 28, the experiment endpoint, the liver and kidneys were harvested to evaluate the impact of possible accumulation of NPs in these organs. Hematoxylin-eosin staining revealed no histopathological signs in the liver and kidneys of non-treated (control, CTR) and treated (RT, NPs and RT+NPs) animals (Fig. S2B), ensuring that these experimental conditions do not compromise animal safety.

3.3. RT in combination with Ch/γ-PGA NPs significantly decreases 4T1 primary tumor growth

We hypothesized that immunostimulatory Ch/γ-PGA NPs administration, in combination with RT, could decrease breast tumor progression. Therefore, we followed primary tumor growth through volume measurements and bioluminescence imaging, as well as, distant metastases formation. Our results showed that tumors grew progressively in the control non-treated animals while the growth of tumors was delayed in treated animals (Fig. 1B). While NPs effect on tumor growth was negligible (432 ± 79 %) comparing to control animals (525 ± 80 %), RT treatment delayed primary tumor growth (333 ± 69 %), although without reaching statistical significance ($p<0.09$). Importantly, the combinatorial treatment of RT+NPs resulted in a significant decrease of tumor growth after 28 days (234 ± 22 %, **, $p<0.003$), potentiating the effect of the single treatments with NPs and RT in 46 % and 30 %, respectively (Fig. 1C). In agreement, we observed that tumors from control animals presented higher weight (0.7 ± 0.2 g) comparing to treated ones. While NPs-treated animals presented a slight decrease in tumor weight (0.5 ± 0.2 g), the RT treatment group significantly exhibited a reduction (0.4 ± 0.1 g; *$p<0.05$). Once again, the combination treatment of RT+NPs further decreased the tumor weight (0.3 ± 0.2 g) in comparison with the non-treated group, although did not reach statistical significance to each of the single treatments (Fig. 1D). These results were corroborated by bioluminescence analysis, which demonstrated that tumors exposed to the combination treatment presented lower bioluminescence, suggesting reduced tumor burden (Fig. 1E). The quantification of bioluminescence through total photon flux (photons/second, p/s) at the primary tumor region showed that NPs slightly impacted tumor burden ($(7.8 \pm 1.4)x10^7$ p/s) comparing to control animals ($(13.0 \pm 2.6)x10^7$ p/s). Importantly, RT treatment decreased tumor bioluminescence

($(6.2 \pm 1.1)x10^7$ p/s), although without reaching statistical significance ($p<0.07$), while only the combination treatment of RT+NPs significantly reduced tumor burden ($(3.2 \pm 1.7)x10^7$ p/s; **,$p<0.01$) (Fig. 1F). In addition, this impairment on tumor growth seems dependent on tumor immunity induced by the combination therapy since NPs alone did not impair the 4T1-Luc proliferation nor migration (Fig. S3A,B). Hematoxylin and eosin staining revealed also that primary tumors from RT+NPs group presented higher necrotic areas in comparison to other groups (Fig. 1G, arrowheads). Overall, these results suggest that the combination therapy of RT+NPs is more efficient in controlling 4T1 breast primary tumor growth.

Figure 1

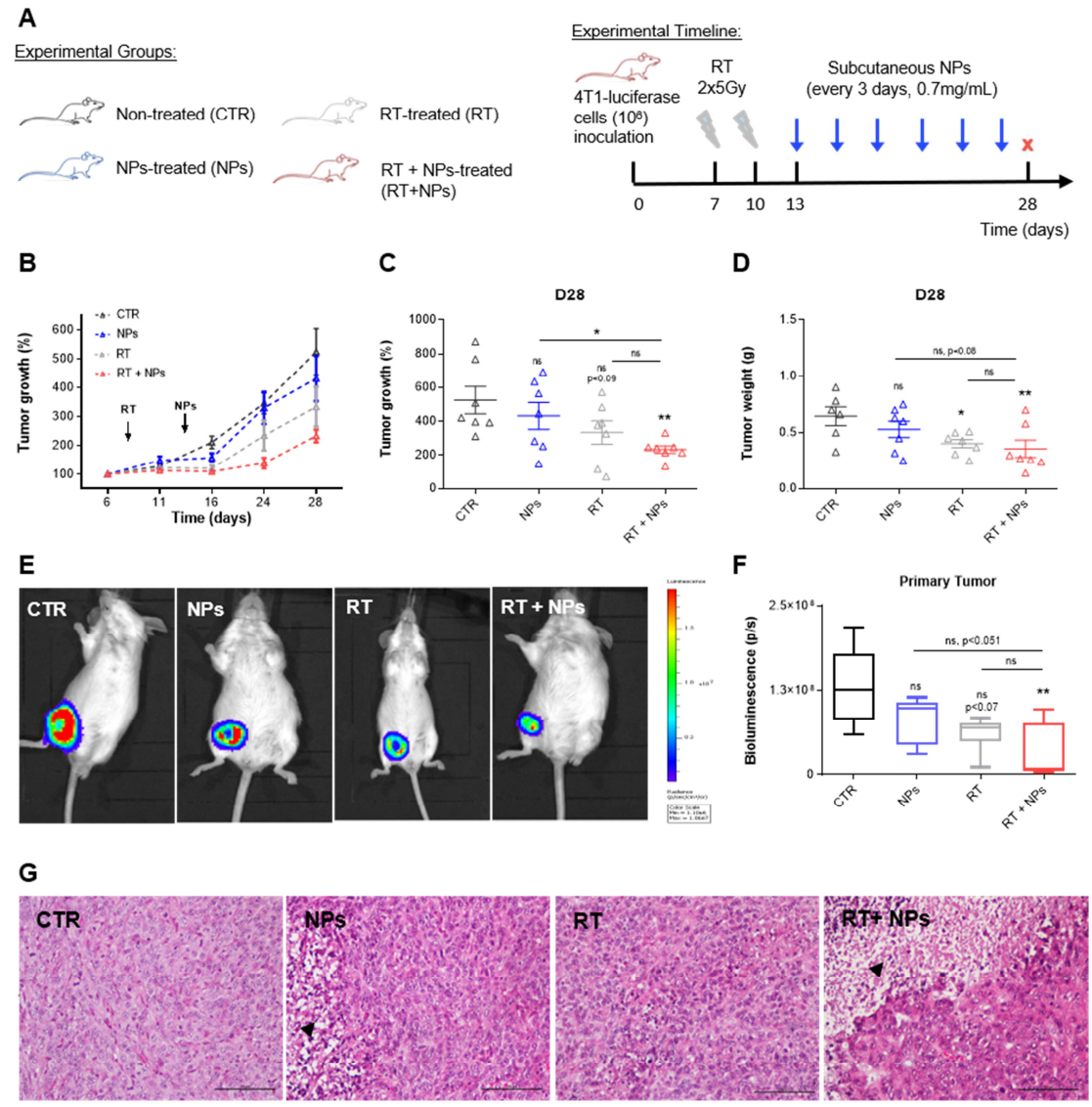

Figure 1. Ch/γ-PGA nanoparticles potentiate radiotherapy effects by decreasing 4T1 primary tumor growth. A. Experimental timeline. BALB/c mice injected with 4T1 cells on the mammary fat pad were submitted to radiotherapy (RT) (2x5 Gy) or treated with Ch/γ-PGA NPs (NPs), or with RT combined with Ch/γ-PGA NPs (RT+NPs). Non-treated animals were used as control (CTR). Animals from RT and RT+NPs group were irradiated at day 7 and day 10 with 5 Gy/fraction. After 3 days, animals from NPs and RT+NPs group were primed with Ch/γ-PGA NPs three times/week for 2 weeks. At the 28th day after tumor cells inoculation, animals were euthanized, and tissues and organs processed for further analysis. **B.** Tumor volume (mm^3) was measured using a caliper and the growth kinetics were normalized to the initial tumor volume for each animal. Based on this, relative (%) tumor growth was estimated. Values represent the average tumor growth of 7 animals and flags represent standard deviation values. **C and D.** Relative (%) tumor growth and tumor weight was measured at the end of experiment, at day 28 (D28). Data show the mean ± SEM. **E.** Mice were bioluminescence imaged to monitor tumor progression. Images were taken 20 minutes after intraperitoneal injection of luciferin. Representative images from D28 are illustrated. **F.** Quantification of total photon flux (the number of photons/second, p/s) at primary tumor region. Median is represented by the horizontal line inside the box plots. **G.** Tumors were processed for histological analysis and stained with hematoxylin and eosin, magnification 200x; scale bar: 100 µm. Data is representative of at least 7 animals per group. Arrows indicate necrotic area. All comparisons were performed using the Kruskal Wallis test followed by Dunn's multiple comparison test ($^{\#}$p<0.05 and **p<0.01 relative to non-treated control or single treatments (NPs or RT)).

3.4. RT in combination with Ch/γ-PGA NPs attenuates spleen leukemoid reaction

The 4T1 model was described to induce a leukemoid reaction associated with granulocytosis and splenomegaly following the injection of 4T1 cells on the mammary fat pad of BALB/c mice. This condition was associated with the systemic release of tumor-derived growth factors [32] and with the appearance of metastatic disease [33]. In agreement, we observed a 9-fold increase in the spleen weight of control animals (CTR, non-treated) by four weeks post-tumor transplant (0.9 ± 0.1 g), in comparison to non-tumor induced animals (healthy, data not shown). Animals treated with NPs or RT had a negligible decrease on spleen weight (0.7 ± 0.2 g or 0.6 ± 0.1 g, respectively) in comparison to control animals (0.9 ± 0.1 g). Notably, combination treatment with RT+NPs presented a reduced spleen weight (0.3 ± 0.1 g) in comparison to control or single-treated animals, probably due to the inhibition of granulocytic hyperplasia (Fig. 2A,B). Additionally, we observed an exuberant reactive hyperplasia in the spleens of control animals where the red and white pulp could not be distinguished. Conversely, the spleens of those animals treated with single therapies, NPs or RT, presented a slight decrease in the hyperplasia condition, and the spleens of the animals submitted to the combination treatment RT+NPs had a near to normal splenic architecture (Fig. 2C). These results evidenced that the combination of RT with NPs administration decreased the leukemoid condition of the 4T1 model, which could be a sign of lower metastatic burden.

Myeloid colony-stimulating factors, namely GM-CSF, G-CSF and M-CSF, previously described to be associated with the leukemoid reaction in the 4T1 model [32], were quantified in the mice serum. Interestingly, there was a clear tendency for a decrease in the levels of GM-CSF in animals treated with NPs or with RT+NPs (9.4 ± 3.4 or 8.0 ± 3.6 pg/mL, respectively) in comparison with control animals (33.3 ± 14.4 pg/mL). Surprisingly, RT treatment did not impact on systemic GM-CSF levels (39.1 ± 17.9 pg/mL) (Fig. 2D). Regarding G-CSF, control animals exhibited a 11-fold increase in comparison to non-tumor induced animals (healthy, data not shown). NPs- and RT-treated animals presented slightly increased G-CSF levels than the control animals, without reaching statistical significance, while RT+NPs treatment significantly increased G-CSF secretion (Fig. 2E). No evident alterations were observed in M-CSF levels in all groups (Fig. 2F). Altogether, the combination of RT with NPs impairs the leukemoid reaction

and the splenomegaly induced by 4T1 cell inoculation, which seems to be partially mediated through myeloid colony-stimulating factors.

Figure 2

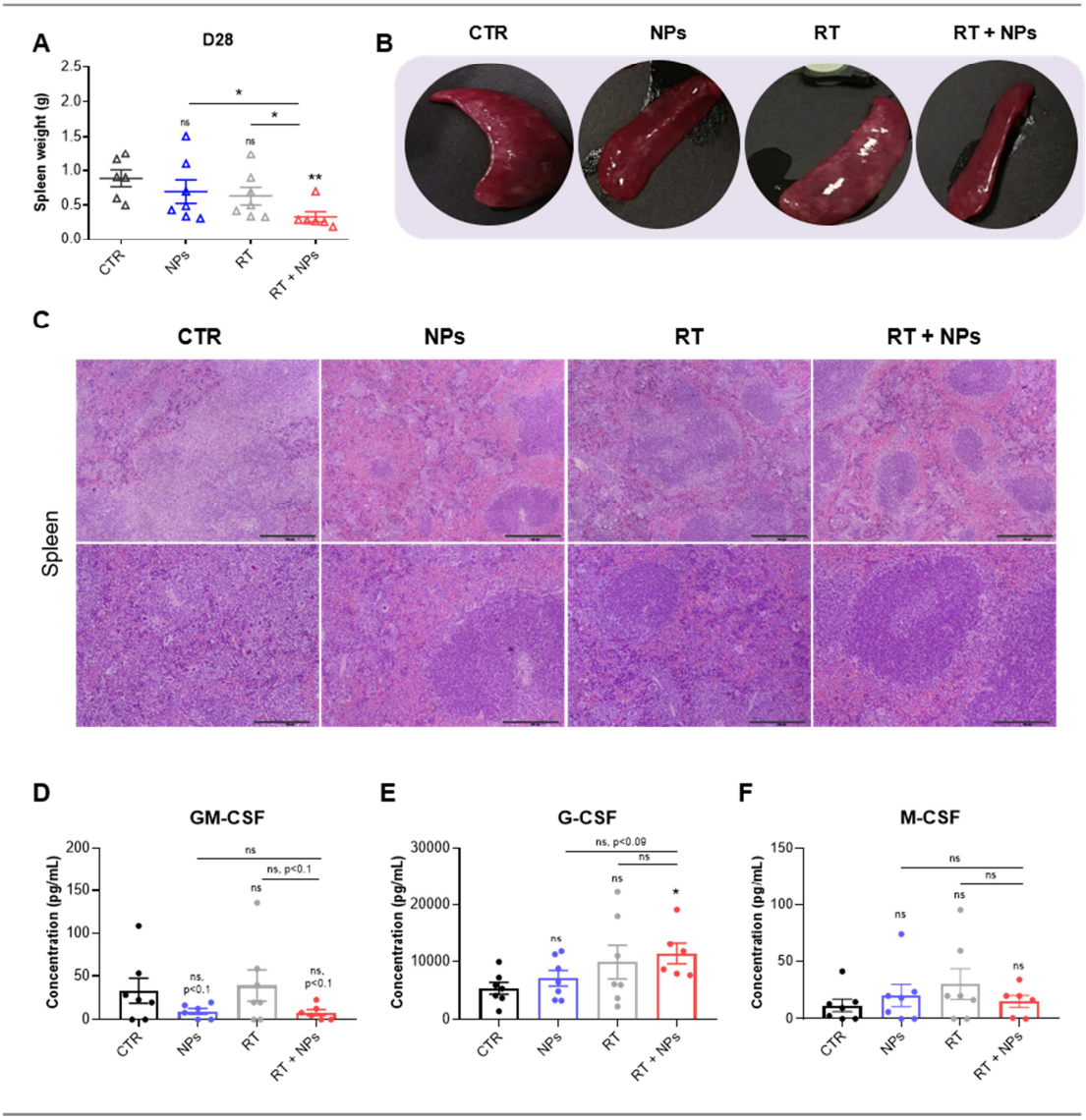

Figure 2. Radiotherapy in combination with Ch/γ-PGA nanoparticles decreases tumor-bearing mice splenomegaly. BALB/c mice injected with 4T1-Luc cells on the mammary fat pad were submitted to radiotherapy (RT) (2x5Gy), treated with Ch/γ-PGA NPs (NPs), or with combination therapy (RT+NPs). Non-treated animals were used as control (CTR). **A.** For each animal, spleen weight was measured at the experimental endpoint, day 28 (D28). Values represent the average spleen weight of 7 animals per group and flags represent standard deviation values. **B.** Representative images of mice spleen. **C.** Spleens were processed for histological procedures and stained with hematoxylin and eosin, magnification 4x; scale bar: 500 µm; magnification 10x; scale bar: 200 µm. Data is representative of at least 7 animals per group. **D-F.** Serum was analyzed at day 28 (D28) through multiplex immunobead assay technology. Outliers were calculated through ROUT method (Q=1%) and removed from the analysis. Data show the mean ± SEM and it is representative of at least 6 animals per group. All comparisons were performed using the Kruskal Wallis test followed by Dunn's multiple comparison test (*p<0.05 and **p<0.01 relative to non-treated control or single treatments (NPs or RT)).

3.5. RT in combination with Ch/γ-PGA nanoparticles decreases the percentage of myeloid cells while increasing T helper 1 response in the spleen

The progression of 4T1 tumors is generally accompanied by a decrease of T cells and an increase in myeloid cells in the spleen [32]. To understand the impact of the combination treatment on the cellular dynamics of the spleen, at day 28, we dissociated spleens from the different groups into single cell suspensions and analyzed, by flow cytometry, the myeloid (Fig. 3A) and lymphoid populations (Fig. 4A). Single treatments (NPs or RT) did not significantly impact the dynamics of myeloid cells in the spleen. However, upon RT+NPs treatment, we found an increase in the percentage of immune cells in the spleen ($CD45^+$), where the percentage of myeloid cells was significantly decreased (Fig. 3B,C). In particular, we observed a significant decrease in the percentage of granulocytic-myeloid derived suppressor cells (MDSCs) ($Ly6G^+$ $Ly6C^-$), while monocytic-MDSCs ($Ly6C^+$ $Ly6G^-$) and neutrophils increased ($Ly6G^+$ $Ly6C^+$) (Fig. 3D-F). These alterations on granulocytic cells and on monocytic-MDSCs were also extended to the primary tumor immune populations (Fig. S4A-E). The percentage of inflammatory macrophages ($F4/80^+$ $Ly6C^+$) was also increased in the spleen upon the combination therapy (Fig. 3G), and the same tendency was observed in the primary tumor (Fig. S4F).

In addition, we observed that single treatments, NPs or RT, had a minor impact on splenic T cell populations (Fig. 4B-G), whereas the combination therapy (RT+NPs) increased the percentage of $CD3^+$ T cells in comparison to the control group (Fig. 4B). Importantly, this increase was only observed in the $CD3^+CD4^+$ and not in $CD3^+CD8^+$ T cells (Fig. 4C), and was associated with an increase in the proportion of IFN-γ-producing $CD3^+CD4^+$ T cells (Fig. 4D). No alterations were observed in the FoxP3-expressing $CD3^+CD4^+$ T cells upon the distinct treatments (Fig. 4E). The frequency of $CD3^+CD8^+$ T cells in the spleen was similar in all treated groups (Fig. 4F). There was a tendency for a higher proportion of IFN-γ-producing $CD3^+CD8^+$ T splenocytes in the animals treated with RT+NPs (Fig. 4G). No significant alterations in the percentage of T cells were observed at the primary tumor site (Fig.S5A-F). Overall, these results suggest that the combinatory therapy of RT with NPs increases T helper 1 ($CD3^+CD4^+IFN\text{-}\gamma^+$ cells) response in the spleen and decreases the percentage of myeloid cells, which may be crucial to impair tumor progression.

Figure 3

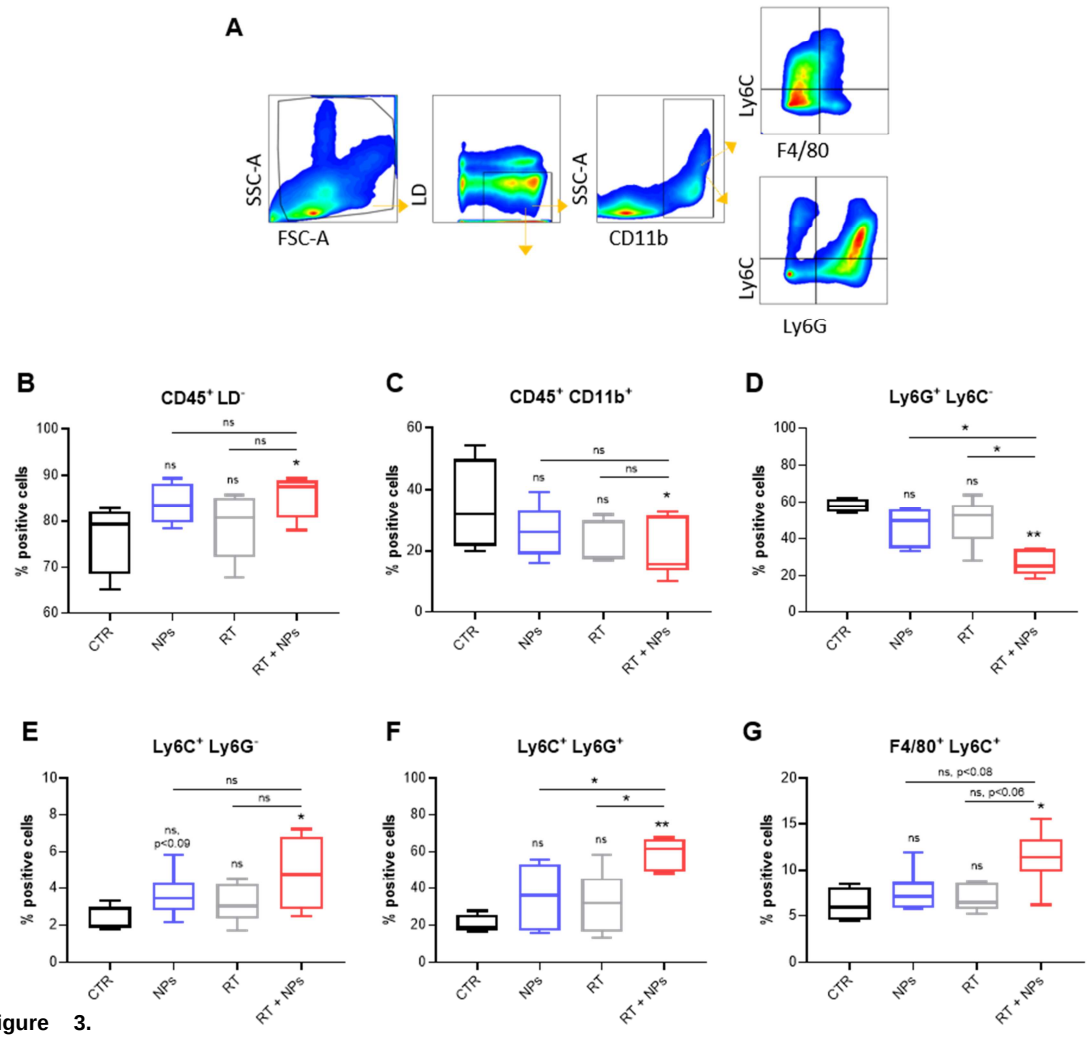

Figure 3.

Radiotherapy in combination with Ch/γ-PGA nanoparticles decreases the percentage of splenic myeloid cells. Mice injected with 4T1 cells on the mammary fat pad were submitted to radiotherapy (RT) (2x5 Gy) or treated with Ch/γ-PGA NPs (NPs), or with combination therapy (RT+NPs). Non-treated animals were used as control (CTR). **A.** At day 28, animals were euthanized, and spleens were collected and processed for flow cytometry analysis. The pseudocolor plots indicate the gate strategy of myeloid cells. $CD45^+$Live Dead $(LD)^-$ cells were gated on single cells (FSC-A vs SSC-H). $CD11b^+$ cells were gated on $CD45^+LD^-$ cells. $F4/80^+Ly6C^+$, $Ly6C^+Ly6G^-$, $Ly6C^-Ly6G^+$, $Ly6C^+Ly6G^+$ cells were gated on $CD11b^+$ cells. **B-G.** The percentage of positive cells was determined. Data is representative of at least 5 animals per group. Median is represented by the horizontal line inside the box plots. All comparisons were performed using the Kruskal Wallis test followed by Dunn's multiple comparison test (*p<0.05, **p<0.01, relative to non-treated control or single treatments (NPs or RT)).

Figure 4

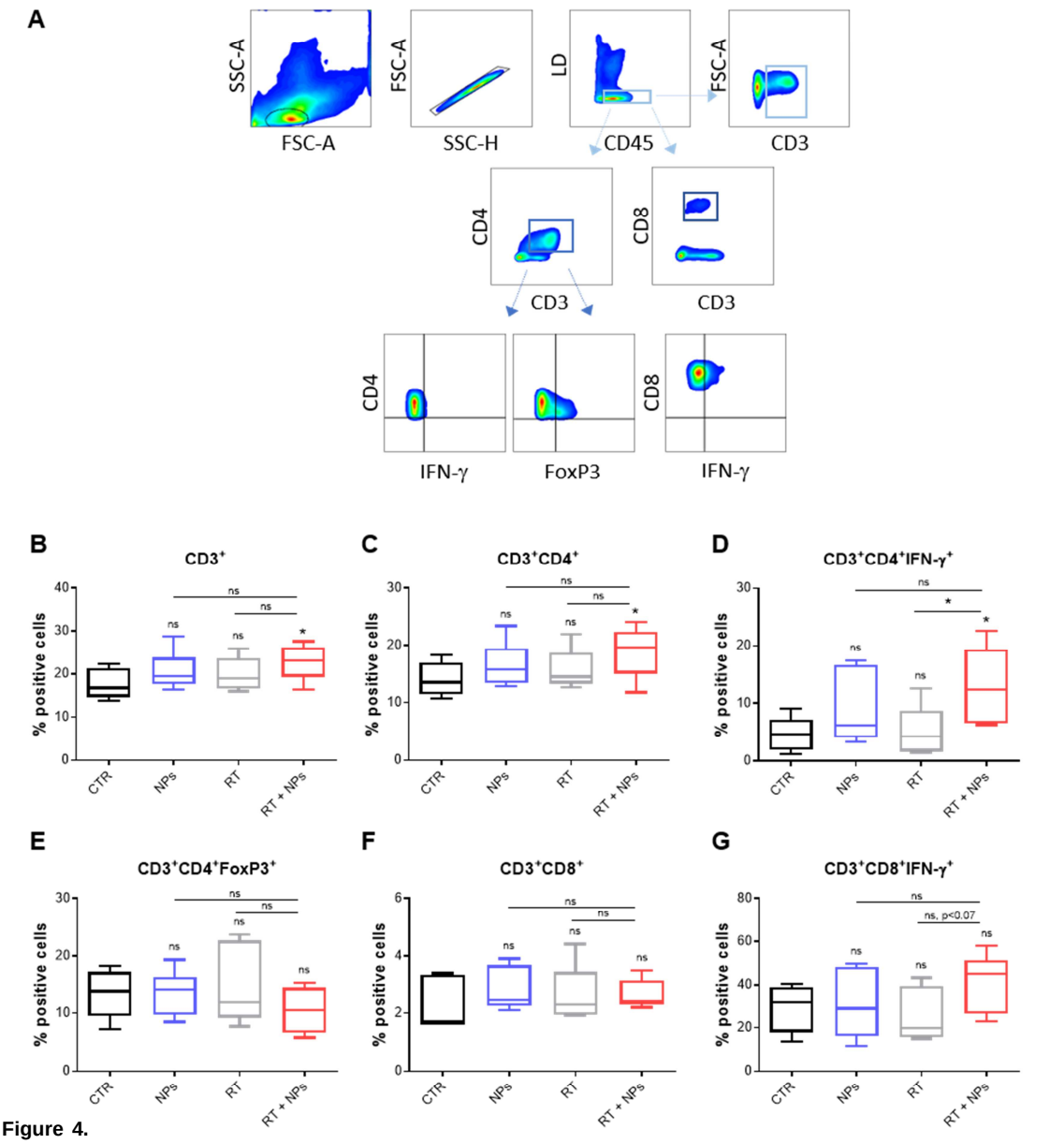

Figure 4.

Radiotherapy in combination with Ch/γ-PGA nanoparticles increases the percentage of splenic CD4 T cells-producing IFN-γ. Mice injected with 4T1-Luc cells were treated with radiotherapy (RT) (2x5 Gy), with Ch/γ-PGA NPs (NPs) or with the combination therapy (RT+NPs). Non-treated animals were used as control (CTR). At day 28, animals were euthanized, and spleens were collected and processed for flow cytometry analysis. **A.** The pseudocolor plots indicate the gate strategy of T cells. $CD45^+$Live Dead $(LD)^-$ cells were gated on single cells (FSC-A vs SSC-H). $CD3^+$, $CD3^+CD4^+$, $CD3^+CD8^+$ T cells were gated on $CD45^+LD^-$ cells. IFN-γ-producing T cells were gated on $CD3^+CD4^+$ or $CD3^+CD8^+$ T cells. FoxP3-expressing cells were gated on $CD3^+CD4^+$ T cells. **B-G.** The percentage of positive cells was determined. Data is representative of at least 5 animals per group. Median is represented by the horizontal line inside the box plots. All comparisons were performed using the Kruskal Wallis test followed by Dunn's multiple comparison test ($^*p<0.05$ relative to non-treated control or single treatments (NPs or RT)).

3.6. RT in combination with Ch/γ-PGA nanoparticles decreases the levels of systemic immunosuppressive cytokines

The production of immune mediators, namely cytokines and chemokines, in the 4T1 model has been explored [34]. To characterize the systemic response, a panel of mouse cytokines and chemokines was evaluated in mice serum through a multiplex analysis. As expected, 4T1 tumor inoculation led to an enhanced expression of cytokines with immunosuppressive and protumor activities, namely, IL-3, IL-4 and IL-10, and the dual player IL-6, in comparison to healthy animals (Fig. 5A). No significant differences were observed between 4T1 tumor-bearing and healthy animals regarding the expression of pro-inflammatory cytokines as IL-12p40, IL-12p70, TNF-α and IFN-γ (Fig. 5B).

Regarding the impact of the different treatments on systemic immunity, we observed an overall decrease of the cytokine levels in the serum of RT+NPs-treated animals, excepting for IL-1α, G-CSF and CCL11 (≥1.5-fold, $p<0.05$), which seemed NPs treatment-dependent (Fig. S6). NPs- and RT+NPs-treated animals presented lower systemic levels of protumor cytokines comparing to control animals, while RT-treated animals presented similar ones (Fig. 5C-F). Specifically, animals treated with RT+NPs had a reduction of 3.5-fold in IL-3 levels, 5.3-fold in IL-4 levels, 13-fold in IL-6 levels and 2.3-fold in IL-10 levels in comparison to RT-treated animals. This combination therapy also potentiated NPs effect, since it decreased 2.1-fold in IL-4 levels, 7-fold in IL-6 levels and 2.3-fold in IL-10 levels, in comparison to NPs-treated animals (Fig. 5C-F). These results suggest that NPs were the major driver in the reduction of immunosuppressive cytokines in the serum of animals treated with RT+NPs, and that RT potentiated this effect. Regarding cytokines with pro-inflammatory activities, we did not observe major alterations in IL-12p40, IL-12p70, TNF-α secretion in RT+NPs-treated animals comparing to control ones. IFN-γ levels were slightly decreased in RT-treated animals ($p<0.09$) while the levels on RT+NPs-treated ones were reestablished (Fig. 5G-J). Overall, these results suggest that the combination therapy RT+NPs has a major impact in the reduction of immunosuppressive and protumor cytokines, which could impact on the phenotype of the myeloid cells in the spleen, tuning the immune cells recruited to the tumor site and, consequently on tumor progression.

Figure 5

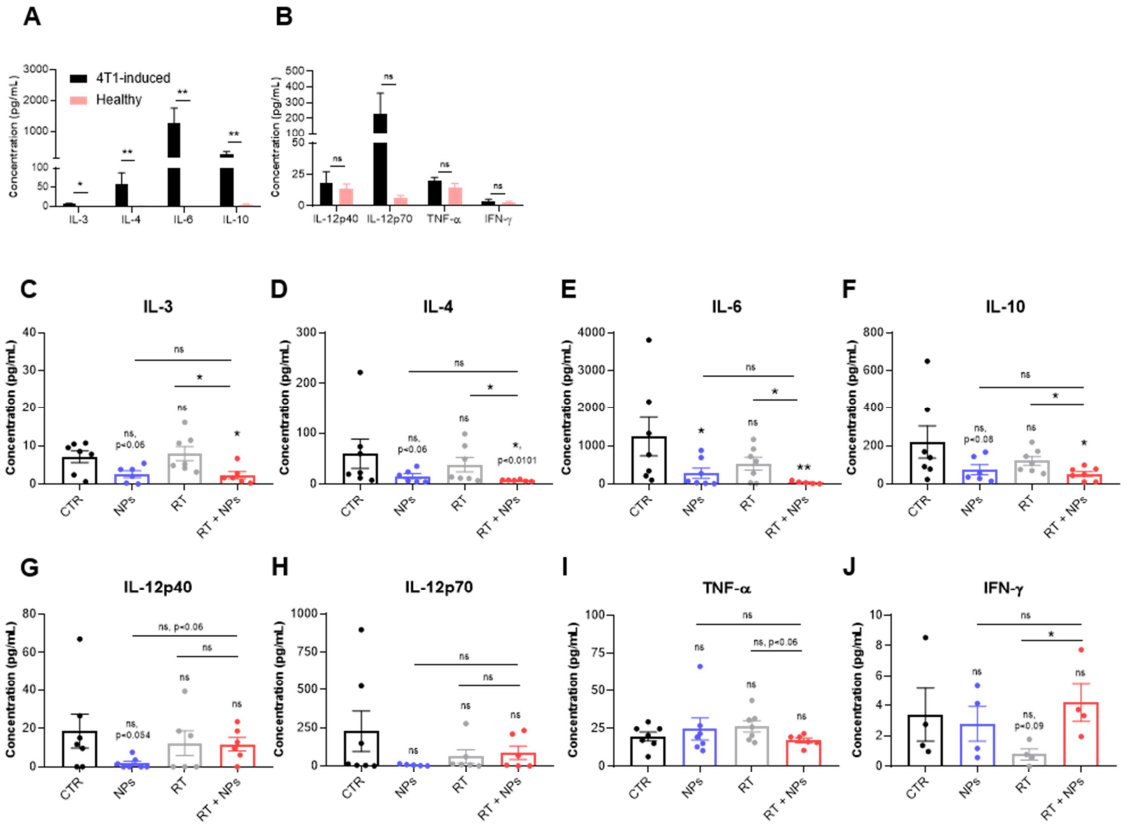

Figure 5. Ch/γ-PGA nanoparticles treatment contributes in higher extension to the decrease of the immunosuppressive cytokines-induced by combination therapy. A. Mice were subcutaneously injected with 4T1-Luc cells and treated as above. At day 28, animals were euthanized, and serum was collected for analysis through Multiplex immunobead assay technology. Outliers were calculated through ROUT method (Q=1%) and removed from the analysis. **A and B.** Serum from non-treated 4T1-induced mice was compared to healthy animals. Data show the mean ± SEM from at least 5 animals per group. Comparisons were performed using the unpaired Mann-Whitney test (*p<0.05, **p<0.01 relative to non-treated animals). **C-J.** All comparisons were performed using the Kruskal Wallis test followed by Dunn's multiple comparison test (*p<0.05, **p<0.01 relative to non-treated control (CTR) or single treatments (NPs or RT)).

3.7. RT in combination with Ch/γ-PGA nanoparticles decreases lung metastasis burden

The poorly immunogenic 4T1 tumor model is highly metastatic to the lungs [31]. Using whole-body fluorescence imaging, animals from different groups were imaged for 4 weeks but no differences regarding the bioluminescence signal in the lungs or in the liver were observed (data not shown). To complement this analysis, we performed hematoxylin and eosin staining of the lungs of treated and non-treated animals. We defined a metastatic score accordingly to the presence or absence of metastatic foci and their size as: absence of foci (score I), small foci (score II), intermediate foci areas (score III) and larger metastasized areas (score IV) (Fig. 6A). NPs treatment and the combination therapy (RT+NPs) significantly reduced lungs metastatic burden (Fig. 6B). Interestingly, we found the largest lung metastasized areas (score III and IV) in non-treated animals (Fig. 6C, D). On animals subjected to NPs treatment, we observed essentially smaller or absent foci (5/7 animals), while RT-treated animals presented small and intermediate lesions (5/7 animals). Notably, the animals from the combination therapy (RT+NPs) exhibited the lowest metastatic burden, essentially represented by scores I and II (6/7 animals) (Fig. 6C, D). These data are consistent with a decrease in the systemic levels of chemotactic molecules, associated with metastases promotion, in the serum of the animals treated with the combination treatment, as CCL4, VEGF and GM-CSF (Fig. 6E, F and Fig. 2D), and also with a decrease of the granulocytic-MDSCs, which are known to prepare the pulmonary metastatic niche and favor the metastatic growth [35, 36]. Altogether, these findings could explain the reduced tumor burden in the lungs of these animals.

Figure 6

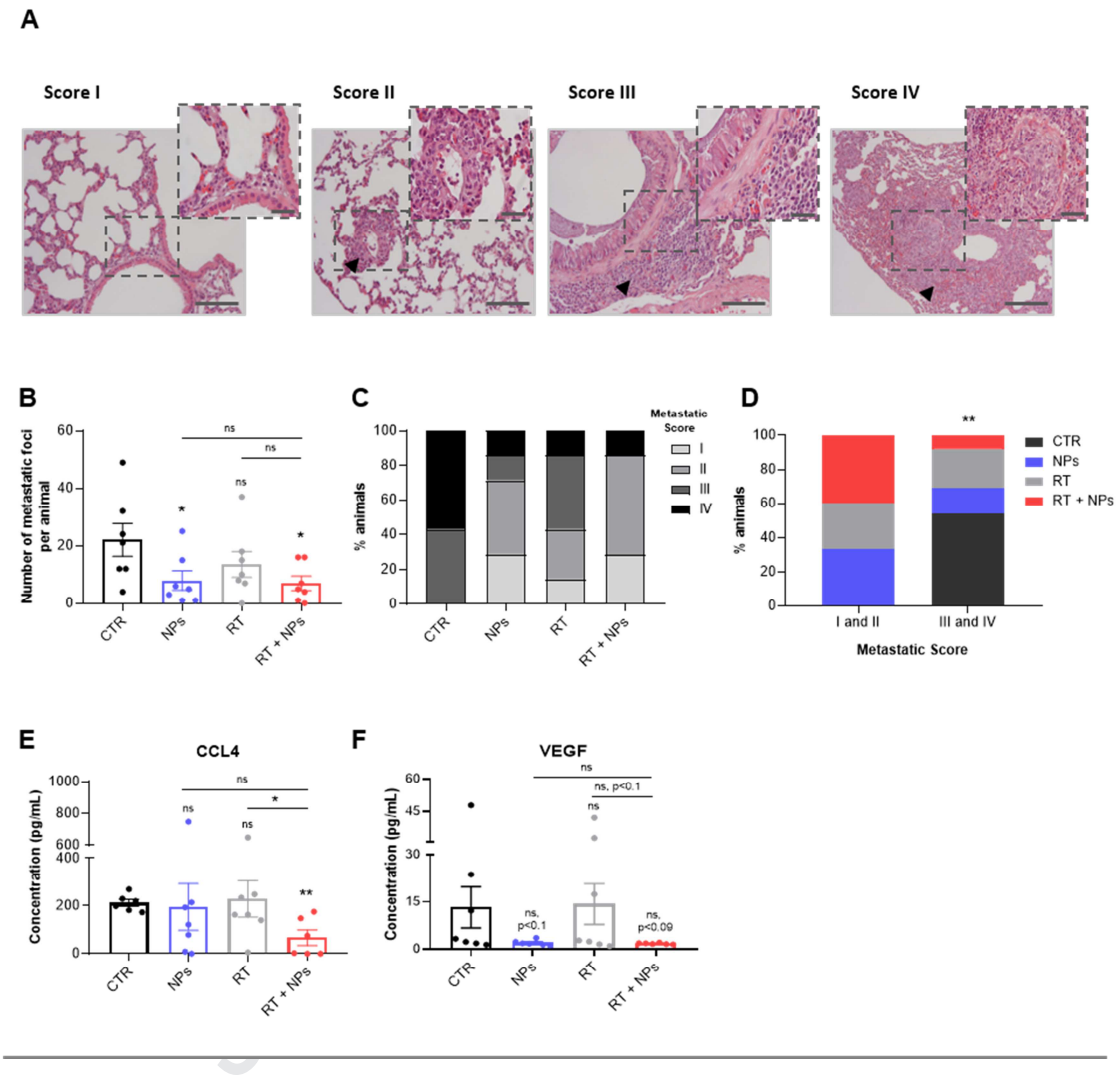

Figure 6. Radiotherapy in combination with Ch/γ-PGA nanoparticles decreases lung metastasis burden. Mice were subcutaneously injected with 4T1-Luc cells and treated as above. At day 28, animals were euthanized, and lungs were recovered for metastases analysis. **A.** Lungs were stained with hematoxylin and eosin, and scored accordingly to the presence or absence of metastatic foci and their size: absent of foci (score I), small metastatic foci (score II), intermediate size foci (score III) and larger areas metastasized (score IV). Arrows indicate metastatic foci. Magnification:200x, scale bar: 100µm; magnification: 600x, scale bar: 30µm. **B.** Quantification of the number of metastatic foci in each animal. Data show the mean ± SEM and it is representative of 7 animals. All comparisons were performed using the Kruskal Wallis test followed by Dunn's multiple comparison test (*p<0.05 relative to non-treated control). **C.** Experimental treatments and respective metastatic score. **D.** The association between treatment with metastatic score I and II vs III and IV was assessed using two-sided Fisher´s exact test (**p<0.008). **E and F.** Serum was analyzed through multiplex immunobead assay technology. Outliers were calculated through ROUT method (Q=1%) and removed from the analysis. Data show the mean ± SEM and it is representative of at least 6 animals. All comparisons were performed using the Kruskal Wallis test followed by Dunn's multiple comparison test (*p<0.05 and **p<0.01 relative to non-treated control or single treatments (NPs or RT)).

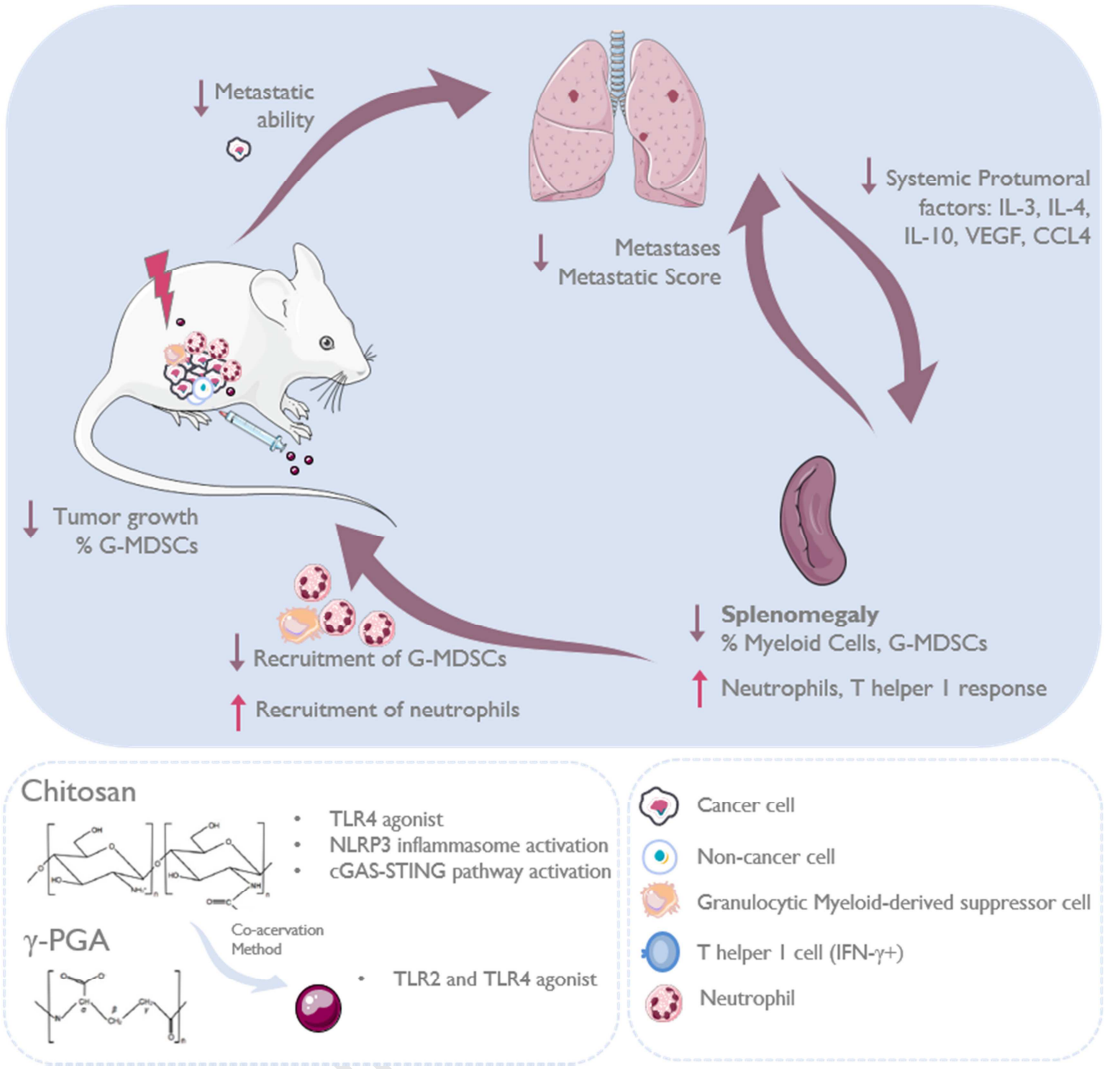

Figure 7 – Schematic of the *in vivo* effects of the therapeutic combination of the Ch/γ-PGA NPs with radiotherapy (2*5Gy) using a 4T1 breast tumor model. Composition of the Ch/γ-PGA NPs and signaling pathways described to be activated by these NPs.

4. DISCUSSION

The main obstacle to anticancer therapy success is the tolerance established during tumor progression by the host [37], which favors the acquisition of an immunosuppressive microenvironment, and consequent resistance to therapies [10, 38, 39]. Therefore, novel anticancer strategies should include immunomodulatory approaches to subvert the tolerance to the tumor. Specifically, RT is known to induce an immunogenic cell death, inducing the appearance of novel antigens and the release of death signals, which promote the activation of the innate immune system and the recruitment of T cells to the tumor site. However, this response will only be effective if the immunosuppressive effects can be overcome. Several efforts have been done to target tumor microenvironment-mediated radioresistance mechanisms [10]. For example, RT followed by insulin-growth factor 1 receptor (IGF-1R) neutralization in orthotopic colorectal cancer models reduced the number of mice with organ metastases [40]. Additionally, preclinical studies have exploited the synergistic effects of RT in combination with immunotherapies, namely anti-PD-1, anti-CTLA-4 and anti-CD25, demonstrating improved therapeutic response [41-43], and are currently in clinical trials [44]. In addition, the emergence of nanomedicine as promising technology for cancer treatment has demonstrated several advantages over conventional therapies in preclinical studies. This includes the improvement of drug therapeutic index by enhancing their specificity, efficacy and/or minimizing the associated adverse effects; enhancement of the pharmaceutical properties (for example, pharmacokinetic and pharmacodynamic profile) of chemotherapeutic agents; ability of sustained or stimulus-triggered drug release; the feasibility of co-delivery of multiple drugs which can be combined with other cancer therapies; the inherent therapeutic properties of some nanomaterials; and the improvement of cost–effectiveness [45]. Nevertheless, a deep understanding of the tumor microenvironment is obligatory to overcome the related obstacles, as the entry and retention of NPs into the tumors, their fate and functionality as well as the challenging clinical translation in humans due to individual differences among patients, and tumors' heterogeneity [46]. Currently, most of the nanostrategies to enhance radiotherapeutic effects relies on the combination with chemotherapeutic agents [47, 48], with several clinical trials ongoing [49]; anti-vascular agents [50]; radiosensitizers such as camptothecin [51], DNA repair inhibitors [52] and Pi3K inhibitors

[53], which are generally very toxic when delivered systemically in their free forms. Also, the use of inorganic NPs as radiosensitizers has been extensively reported [54, 55], despite remaining a challenge for clinical translation. Advances in immunotherapy research have resulted in many immunomodulatory nanostrategies, being inert NPs-delivering immune stimulating agents [56, 57], functionalized-NPs with antibodies [58], and combination therapeutic strategies [59, 60] the main deliverables. However, the inherent immunostimulatory/ therapeutic features of some natural materials to strength radiotherapy is not deeply explored.

In the current preclinical study, we tested the combination of conventional RT with a nanomedicine-based approach, using the immunostimulatory Ch/γ-PGA NPs [24, 26] for the treatment of metastatic triple-negative breast cancer. For that, we used a mouse model that closely mimics the traits of human disease, with cancer cells systemically metastasizing to lungs. This therapeutic combination has never been explored before, and the current data provide the proof-of-concept that it can significantly elicit an antitumor immunity likely by breaking down the immunosuppressive microenvironment. The therapeutic advantage obtained through the combination of RT with the Ch/γ-PGA NPs resulted from the synergistic effects of each single treatments in potentiating the antitumor immunity. Whereas RT slightly decreased primary tumor burden, Ch/γ-PGA NPs attenuated the systemic immunosuppression. Additionally, we only observed a decrease in the percentage of myeloid cells and an increase in $CD4^+$ T cell response in the spleen of animals submitted to the combination therapy, which suggests that such treatment promotes the antitumor immunity (Fig. 7). Curiously, single treatments were not enough to promote T cell activation neither their infiltration into the tumor, probably due to the immunosuppressive environment created by the established 4T1 tumors. Accordingly, it is known that primary 4T1 tumors are constituted by a high percentage of myeloid cells ($Gr1b^+$ $CD11b^+$), which generally sustain tumor progression [31, 36]. These cells can inhibit T cell activities [61], sustain an immunosuppressive environment and promote lung metastases formation [36].

When exploiting the underlying mechanisms, we observed that only the combination therapy triggered significant alterations in splenic $CD11b^+$ cells, with a decrease in granulocytic-MDSCs and an increase in neutrophils and monocytic-MDSCs. This myeloid cell reduction can be associated to the splenic leukemoid reaction attenuation and of the reduction of cytokine levels

in the serum, specifically IL-3, IL-6, GM-CSF and VEGF, which impact myeloid differentiation [62, 63]. These data are in accordance with other studies that showed an association between leukemoid reaction and breast cancer progression [33]. Additionally, we noticed that the combination of Ch/γ-PGA NPs with RT changes the major cellular players- granulocytic-MDSCs - towards neutrophils and inflammatory macrophages. In fact, it was described that granulocytic-MDSCs are frequently associated with poor disease progression, supporting metastasis establishment [36], while the role of neutrophils is still questionable, depending of the tumor type, their abundance and profile. Although neutrophils have been shown to promote metastasis in breast cancer [64], there is also evidence that they inhibit lung metastatic seeding through H_2O_2 production [65]. More recently, Takeshima *et al.,* evidenced that RT combined with G-CSF administration induced neutrophils with enhanced reactive oxygen species production, improving RT-mediated antitumor activities [66]. Thus, the accumulation of neutrophils might also explain the better outcome of the animals treated with the combination therapy.

Importantly, the combination of RT and Ch/γ-PGA NPs decreased lung metastasis in a NPs treatment-dependent way. This reduction can also be partially mediated by a diminished immunosuppressive (IL-3, IL-4, IL-6, IL-10) environment (Fig. 7). In fact, others have shown the impact of these cytokines on the metastatic process. For example, RNAi-mediated silencing of IL-4Rα, a component of the IL-4 receptor, was enough to reduce metastases growth in mammary tumor models. Similar results were obtained in IL-4-deficient mice [67]. Others demonstrated that targeting IL-4 signaling sensitized breast cancer cells to anticancer therapy and strengthened immune responses by increasing $CD8^+$ T cells-expressing IFN-γ [68]. IL-6/JAK/STAT3 axis has been associated with tumor progression and metastasis [69] and a variant of IL-6 is associated with metastasis in breast cancer patients [70]. IL-10 levels in the serum have also been associated with poor prognosis in several types of cancer [71]. Additionally, the decrease in pro-angiogenic factors, as IL-3 and VEGF, might be contributing to the reduction of metastasis observed in the animals treated with NPs or with the combination therapy. In fact, IL-3 targeting was described to hamper tumor vessels formation [72], while VEGF inhibition associated with the suppression of breast cancer metastasis [73]. Moreover, high VEGF levels induce defective DC development and function and, are associated with and increased production of B cells and immature $Gr\text{-}1^+$ myeloid cells, promoting abortive

myelopoiesis and systemic accumulation of MDSCs [63]. Importantly, CCL4 is reduced in the serum of animals treated with our combination therapy, and this chemokine has been associated with breast cancer metastasis to bone [74]. Altogether, the reduction of immunosuppressive and protumor mediators was associated with lower metastatic burden of the animals treated with the combination therapy or single NPs (Fig. 7).

Other studies combining RT with immunotherapeutic approaches have reported synergistic effects. Demaria and colleagues' studies using a single dose of 12 Gy, in the presence or absence of anti-CTLA-4, showed a delay in the growth of 4T1 irradiated tumors, although no statistical differences were observed between RT- or RT+anti-CTLA-4-treated animals. Additionally, animals treated with RT+anti-CTLA-4 had an increased survival comparing to single treated animals, and this was correlated with inhibition of lung metastasis [41], which suggests that both treatments synergize to potentiate the antitumor response. The RT immunogenic effects are described to be dependent of TLR4 activation in DCs, and patients with breast cancer carrying a TLR4 loss-of-function allele relapse more rapidly after RT than those carrying the normal allele [75]. The exact mechanism by which RT and NPs are synergizing will likely occur via activation of Toll-like receptors 2 and 4, triggering innate immunity and activating a pro-inflammatory immune response, as already suggested by other authors [75-78]. Still, further studies will need to be conducted before translating this knowledge to clinical studies. In fact, both Ch-NPs and γ-PGA-NPs have been described to induce DCs activation through TLR4- and TLR2-dependent mechanisms [76-78], and we have previously demonstrated that Ch/γ-PGA NPs can revert immunosuppressive macrophages (IL-10-treated) and immature DCs towards an immunostimulatory profile *in vitro* [24]. This observation is in agreement with the decrease of systemic immunosuppressive cytokines in NPs-treated animals [24]. Furthermore, pro-/anti-inflammatory cytokines ratio was increased, possibly contributing to the delayed primary tumor growth and lung metastasis burden.

Furthermore, some strategies involving inorganic NPs combined with immune stimulants and/or tumor antigens to potentiate RT have been recently explored. Patel and colleagues developed NPs constituted by an inner polyplex core composed of PC7A and CpG oligodeoxynucleotide (Toll-like receptor (TLR) 9), and an outer layer composed of a bacterial membrane, modified on its surface with maleimide groups to enhance antigen uptake. These NPs, when combined with

RT (12 Gy, single dose), resulted in activation of DCs and effector T cells, marked tumor regression, and tumor-specific antitumor immune memory [79]. Also, Chen and co-workers developed core-shell nanoparticles based on poly(lactic-co-glycolic) acid (PLGA) encapsulating water-soluble catalase (Cat), an enzyme able to decompose H_2O_2 in O_2, and loading Imiquimod, a TLR 7 agonist, within the PLGA shell. These NPs combined with anti-CTLA-4 enhanced RT (8 Gy, single dose) efficacy by relieving the tumor hypoxia and modulating the immunosuppressive tumor microenvironment [56]. In our study, Ch/γ-PGA NPs exert their intrinsic immunostimulatory capacity and potentiate RT effects, without additional immunostimulatory agents. In fact, these Ch/γ-PGA NPs can act as agonists for TLR2, TLR4 and likely as activators of NLRP3 inflammasome [80], making them excellent biomaterials to use in combination therapies. Their combination with RT was enough to significantly reduce tumor growth and lung metastasis burden, but their ability to prevent cancer recurrence was not addressed. Additionally, this combination therapy reduced the secretion of immunosuppressive factors, without additional treatment with immune checkpoint inhibitors, as anti-CTLA-4. Thus, our data suggest that RT+NPs can more efficiently prime an adaptive immune response when compared to RT alone, triggering whole-body systemic immunotherapeutic effects.

Behind their impact on immune response, Ch/γ-PGA NPs were described to be internalized through caveolae-dependent, related with the lipid raft-mediated route, but not through the inhibition of invagination of caveolae. Also, Ch/γ-PGA NPs internalization can occur via micropinocytosis, despite its minor role. Importantly, the lower percentage of co-localization of Ch/DNA/γ-PGA NPs with lysosomes when compared with their Ch/DNA NPs [81] underlines the γ-PGA worth for these strategies. In addition, it has been reported that macropinosomes can acidify but do not intersect with lysosomes, thus representing an alternative cell entry route of NPs for the avoidance of lysosomal degradation [82]. Overall, Ch/γ-PGA NPs present the ability to escape this defense mechanism, being able to act on intracellular signaling pathways, as the activation of cGAS-STING, leading to the enhanced transcription of IFN-γ-responsive genes [83].

Despite their huge potential as adjuvants to anticancer therapies, Ch and γ-PGA formulations have some manageable challenges [84]. While the Ch and γ-PGA biological effects are dependent on the source, purity, molecular weight (MW) and type of formulation, Ch degree of

deacetylation also impacts its physicochemical and immunological characteristics and, as a consequence, host immune responses [85, 86]. Also, Lee and colleagues showed that type I interferon response is dependent on γ-PGA MW through CD14/TLR4-MD2 complex activation [87]. On the other hand, the influence of Ch MW on immune response remains contradictory likely due to the ambiguous classification of low and high MW. While some authors claim that low MW chitosan (10 kDa) is more effective in immune system stimulation than high MW chitosan (300 kDa) [88], others show that MW around 300 kDa has a greater immunostimulatory effect than a low MW [89]. Furthermore, different sources of γ-PGA can strongly impact the host immune response [90] as well as Ch sources [91]. Thus, the advances on this area can undergo to the standardization of nanoformulation composition, ensuring the reproducibility of the preparation to obtain the desired biological effect.

In summary, the present study demonstrates that it is possible to achieve a systemic therapeutic immune response against a poorly immunogenic and spontaneously metastasizing mammary carcinoma through the combination of primary tumor irradiation with Ch/γ-PGA NPs local administration. This technically simple and relatively low cost radioimmunotherapy benefits from the immunogenic potential of RT and from the intrinsic immunomodulatory properties of Ch/γ-PGA NPs, establishing the basis for a novel therapeutic combination. In the near future, these NPs may also be exploited as carriers for specific drugs, proteins [26], peptides or targeted antibodies to deliver at both primary and metastatic sites.

Acknowledgments

This work was financially supported by FEDER – Fundo Europeu de Desenvolvimento Regional funds through the COMPETE 2020 – Operacional Programme for Competitiveness and Internationalisation (POCI), Portugal 2020, by Portuguese funds through FCT –Fundação para a Ciência e a Tecnologia/Ministério da Ciência, Tecnologia e do Ensino Superior in the framework of the project “MAGICIAM-a MAcrophaGe Immunomodulatory-delivery system to prevent Cancer Invasion And Metastasis” (PTDC/BTM-SAL/31859/2017) and by Fund for Scientific Research Flanders (FWO-Vlaanderen). Some human resources were supported through the FCT PhD Programmes and by the Human Capital Operational Programme (POCH), specifically by the BiotechHealth Programme. F. Castro (PD/BD/114013/2015), M.L. Pinto

(PD/BD/81103/2011), C.L. Pereira (SFRH/BD/85779/2012), K Serre (FCT Investigator Starting Grant IF/00004/2014); R.M. Gonçalves (FCT Investigator Starting Grant IF/00638/2014) and M.J. Oliveira (FCT2012-Investigator Program IF/01066/2012) also acknowledge FCT for their funding. The authors would also like to acknowledge Claúdia Machado and Nuno Mendes for the assistance with histological processing, Rui Fernandes for the support with TEM analysis, and the support of the i3S Scientific Platform Histology and Electron Microscopy Unit (HEMS), member of the PPBI (PPBI-POCI-01-0145-FEDER-022122). The authors also acknowledge Biointerfaces and Nanotechnology (BN) core facility with the assistance in FTIR by Ricardo Vidal.

Author Contributions

FC was responsible for conceptualization, methodology, investigation, formal analysis, and writing of original draft ; MLP was involved in conceptualization, formal analysis, and writing - review & editing; CLP and FG was participated in the methodology and writing - review & editing; KS, MAB and KV provided resources and writing - review & editing; RMG and OdW were involved in the supervision, providing resources, and writing - review & editing and MJO was responsible for conceptualization, supervision, funding acquisition, project administration and writing - review & editing.

Availability of data and materials

The majority of the data obtained, and the materials used are included in this publication or in the supplementary material. Additional data or materials will be provided upon reasonable request and the signing of a material transfer agreement.

5. REFERENCES

[1] J. Thariat, J.M. Hannoun-Levi, A. Sun Myint, T. Vuong, J.P. Gerard, Past, present, and future of radiotherapy for the benefit of patients, Nat Rev Clin Oncol 10(1) (2013) 52-60.

[2] E.B. Golden, L. Apetoh, Radiotherapy and immunogenic cell death, Semin Radiat Oncol 25(1) (2015) 11-7.

[3] H. Kono, K.L. Rock, How dying cells alert the immune system to danger, Nature reviews. Immunology 8(4) (2008) 279-89.

[4] S.V. Kozin, W.S. Kamoun, Y. Huang, M.R. Dawson, R.K. Jain, D.G. Duda, Recruitment of Myeloid but not Endothelial Precursor Cells Facilitates Tumor Regrowth after Local Irradiation, Cancer Res 70(14) (2010) 5679-5685.

[5] R.R. Weichselbaum, H. Liang, L. Deng, Y.X. Fu, Radiotherapy and immunotherapy: a beneficial liaison?, Nat Rev Clin Oncol 14(6) (2017) 365-379.

[6] J. Xu, J. Escamilla, S. Mok, J. David, S. Priceman, B. West, G. Bollag, W. McBride, L. Wu, CSF1R signaling blockade stanches tumor-infiltrating myeloid cells and improves the efficacy of radiotherapy in prostate cancer, Cancer Res 73(9) (2013) 2782-94.

[7] E.L. Kuan, S.F. Ziegler, A tumor–myeloid cell axis, mediated via the cytokines IL-1α and TSLP, promotes the progression of breast cancer, Nat Immunol 19(4) (2018) 366-374.

[8] S.K. Bunt, L. Yang, P. Sinha, V.K. Clements, J. Leips, S. Ostrand-Rosenberg, Reduced Inflammation in the Tumor Microenvironment Delays the Accumulation of Myeloid-Derived Suppressor Cells and Limits Tumor Progression, Cancer Res 67(20) (2007) 10019-10026.

[9] B.Z. Qian, J.W. Pollard, Macrophage diversity enhances tumor progression and metastasis, Cell 141(1) (2010) 39-51.

[10] H.E. Barker, J.T. Paget, A.A. Khan, K.J. Harrington, The tumour microenvironment after radiotherapy: mechanisms of resistance and recurrence, Nat Rev Cancer 15(7) (2015) 409-25.

[11] Y. Zhu, B.L. Knolhoff, M.A. Meyer, T.M. Nywening, B.L. West, J. Luo, A. Wang-Gillam, S.P. Goedegebuure, D.C. Linehan, D.G. DeNardo, CSF1/CSF1R Blockade Reprograms Tumor-Infiltrating Macrophages and Improves Response to T-cell Checkpoint Immunotherapy in Pancreatic Cancer Models, Cancer Res 74(18) (2014) 5057-5069.

[12] M.A. Cannarile, M. Weisser, W. Jacob, A.M. Jegg, C.H. Ries, D. Ruttinger, Colony-stimulating factor 1 receptor (CSF1R) inhibitors in cancer therapy, J Immunother Cancer 5(1) (2017) 53.

[13] V. Kumar, L. Donthireddy, D. Marvel, T. Condamine, F. Wang, S. Lavilla-Alonso, A. Hashimoto, P. Vonteddu, R. Behera, M.A. Goins, C. Mulligan, B. Nam, N. Hockstein, F. Denstman, S. Shakamuri, D.W. Speicher, A.T. Weeraratna, T. Chao, R.H. Vonderheide, L.R. Languino, P. Ordentlich, Q. Liu, X. Xu, A. Lo, E. Pure, C. Zhang, A. Loboda, M.A. Sepulveda, L.A. Snyder, D.I. Gabrilovich, Cancer-Associated Fibroblasts Neutralize the Anti-tumor Effect of CSF1 Receptor Blockade by Inducing PMN-MDSC Infiltration of Tumors, Cancer cell 32(5) (2017) 654-668.

[14] V. Fleming, X. Hu, R. Weber, V. Nagibin, C. Groth, P. Altevogt, J. Utikal, V. Umansky, Targeting Myeloid-Derived Suppressor Cells to Bypass Tumor-Induced Immunosuppression, Front Immunol 9(398) (2018).

[15] A. Mantovani, F. Marchesi, A. Malesci, L. Laghi, P. Allavena, Tumour-associated macrophages as treatment targets in oncology, Nat Rev Clin Oncol 14(7) (2017) 399-416.

[16] A. Teresa Pinto, M. Laranjeiro Pinto, A. Patrícia Cardoso, C. Monteiro, M. Teixeira Pinto, A. Filipe Maia, P. Castro, R. Figueira, A. Monteiro, M. Marques, M. Mareel, S.G. dos Santos, R.

Seruca, M. Adolfo Barbosa, S. Rocha, M. José Oliveira, Ionizing radiation modulates human macrophages towards a pro-inflammatory phenotype preserving their pro-invasive and pro-angiogenic capacities, Sci Rep 6 (2016) 18765.

[17] M. Luo, H. Wang, Z. Wang, H. Cai, Z. Lu, Y. Li, M. Du, G. Huang, C. Wang, X. Chen, M.R. Porembka, J. Lea, A.E. Frankel, Y.X. Fu, Z.J. Chen, J. Gao, A STING-activating nanovaccine for cancer immunotherapy, Nat Nanotechnol 12(7) (2017) 648-654.

[18] R. Kuai, L.J. Ochyl, K.S. Bahjat, A. Schwendeman, J.J. Moon, Designer vaccine nanodiscs for personalized cancer immunotherapy, Nat Mater 16 (2016) 489.

[19] Y. Min, K.C. Roche, S. Tian, M.J. Eblan, K.P. McKinnon, J.M. Caster, S. Chai, L.E. Herring, L. Zhang, T. Zhang, J.M. DeSimone, J.E. Tepper, B.G. Vincent, J.S. Serody, A.Z. Wang, Antigen-capturing nanoparticles improve the abscopal effect and cancer immunotherapy, Nat Nanotechnol 12(9) (2017) 877-882.

[20] A.W. Li, M.C. Sobral, S. Badrinath, Y. Choi, A. Graveline, A.G. Stafford, J.C. Weaver, M.O. Dellacherie, T.-Y. Shih, O.A. Ali, J. Kim, K.W. Wucherpfennig, D.J. Mooney, A facile approach to enhance antigen response for personalized cancer vaccination, Nat Mater 17(6) (2018) 528-534.

[21] G. Zhu, L. Mei, H.D. Vishwasrao, O. Jacobson, Z. Wang, Y. Liu, B.C. Yung, X. Fu, A. Jin, G. Niu, Q. Wang, F. Zhang, H. Shroff, X. Chen, Intertwining DNA-RNA nanocapsules loaded with tumor neoantigens as synergistic nanovaccines for cancer immunotherapy, Nat Commun 8(1) (2017) 1482.

[22] L.M. Kranz, M. Diken, H. Haas, S. Kreiter, C. Loquai, K.C. Reuter, M. Meng, D. Fritz, F. Vascotto, H. Hefesha, C. Grunwitz, M. Vormehr, Y. Hüsemann, A. Selmi, A.N. Kuhn, J. Buck, E. Derhovanessian, R. Rae, S. Attig, J. Diekmann, R.A. Jabulowsky, S. Heesch, J. Hassel, P. Langguth, S. Grabbe, C. Huber, Ö. Türeci, U. Sahin, Systemic RNA delivery to dendritic cells exploits antiviral defence for cancer immunotherapy, Nature 534 (2016) 396-401.

[23] R. Kuai, X. Sun, W. Yuan, L.J. Ochyl, Y. Xu, A. Hassani Najafabadi, L. Scheetz, M.Z. Yu, I. Balwani, A. Schwendeman, J.J. Moon, Dual TLR agonist nanodiscs as a strong adjuvant system for vaccines and immunotherapy, J Control Release 282 (2018) 131-139.

[24] F. Castro, M.L. Pinto, A.M. Silva, C.L. Pereira, G.Q. Teixeira, M. Gomez-Lazaro, S.G. Santos, M.A. Barbosa, R.M. Goncalves, M.J. Oliveira, Pro-inflammatory chitosan/poly(gamma-glutamic acid) nanoparticles modulate human antigen-presenting cells phenotype and revert their pro-invasive capacity, Acta Biomater 63 (2017) 96-109.

[25] C.L. Pereira, J.C. Antunes, R.M. Goncalves, F. Ferreira-da-Silva, M.A. Barbosa, Biosynthesis of highly pure poly-gamma-glutamic acid for biomedical applications, J Mater Sci Mater Med 23(7) (2012) 1583-91.

[26] F. Castro, M.L. Pinto, R. Almeida, F. Pereira, A.M. Silva, C.L. Pereira, S.G. Santos, M.A. Barbosa, R.M. Goncalves, M.J. Oliveira, Chitosan/poly(gamma-glutamic acid) nanoparticles incorporating IFN-gamma for immune response modulation in the context of colorectal cancer, Biomater Sci 7(8) (2019) 3386-3403.

[27] R.M. Goncalves, A.C. Pereira, I.O. Pereira, M.J. Oliveira, M.A. Barbosa, Macrophage response to chitosan/poly-(gamma-glutamic acid) nanoparticles carrying an anti-inflammatory drug, J Mater Sci Mater Med 26(4) (2015) 167.

[28] J.C. Antunes, C.L. Pereira, G.Q. Teixeira, R.V. Silva, J. Caldeira, S. Grad, R.M. Goncalves, M.A. Barbosa, Poly(gamma-glutamic acid) and poly(gamma-glutamic acid)-based nanocomplexes enhance type II collagen production in intervertebral disc, J Mater Sci Mater Med 28(1) (2017) 6.

[29] C. Cunha, Q.T. G, C. Ribeiro-Machado, L.P. C, J.R. Ferreira, M. Molinos, G.S. S, M.A. Barbosa, M.G. R, Modulation of the In Vivo Inflammatory Response by Pro- Versus Anti-Inflammatory Intervertebral Disc Treatments, Int J Mol Sci 21(5) (2020) 1730.

[30] J.C. Antunes, C.L. Pereira, M. Molinos, F. Ferreira-da-Silva, M. Dessi, A. Gloria, L. Ambrosio, R.M. Goncalves, M.A. Barbosa, Layer-by-layer self-assembly of chitosan and poly(gamma-glutamic acid) into polyelectrolyte complexes, Biomacromolecules 12(12) (2011) 4183-95.

[31] S.A. DuPre, D. Redelman, K.W. Hunter, Jr., The mouse mammary carcinoma 4T1: characterization of the cellular landscape of primary tumours and metastatic tumour foci, Int J Exp Pathol 88(5) (2007) 351-60.

[32] S.A. DuPre, K.W. Hunter, Jr., Murine mammary carcinoma 4T1 induces a leukemoid reaction with splenomegaly: association with tumor-derived growth factors, Exp Mol Pathol 82(1) (2007) 12-24.

[33] J. Steenbrugge, K. Breyne, K. Demeyere, O. De Wever, N.N. Sanders, W. Van Den Broeck, C. Colpaert, P. Vermeulen, S. Van Laere, E. Meyer, Anti-inflammatory signaling by mammary tumor cells mediates prometastatic macrophage polarization in an innovative intraductal mouse model for triple-negative breast cancer, J Exp Clin Cancer Res 37(1) (2018) 191.

[34] W.H. Walker Ii, J.C. Borniger, Surbhi, A.A. Zalenski, S.L. Muscarella, J.A. Fitzgerald, N. Zhang, M.M. Gaudier-Diaz, A.C. DeVries, Mammary Tumors Induce Central Pro-inflammatory Cytokine Expression, but Not Behavioral Deficits in Balb/C Mice, Sci Rep 7(1) (2017) 8152.

[35] M. Kowanetz, X. Wu, J. Lee, M. Tan, T. Hagenbeek, X. Qu, L. Yu, J. Ross, N. Korsisaari, T. Cao, H. Bou-Reslan, D. Kallop, R. Weimer, M.J. Ludlam, J.S. Kaminker, Z. Modrusan, N. van Bruggen, F.V. Peale, R. Carano, Y.G. Meng, N. Ferrara, Granulocyte-colony stimulating factor promotes lung metastasis through mobilization of Ly6G+Ly6C+ granulocytes, Proc Natl Acad Sci U S A 107(50) (2010) 21248-55.

[36] M. Ouzounova, E. Lee, R. Piranlioglu, A. El Andaloussi, R. Kolhe, M.F. Demirci, D. Marasco, I. Asm, A. Chadli, K.A. Hassan, M. Thangaraju, G. Zhou, A.S. Arbab, J.K. Cowell, H. Korkaya, Monocytic and granulocytic myeloid derived suppressor cells differentially regulate spatiotemporal tumour plasticity during metastatic cascade, Nat Commun 8 (2017) 14979.

[37] A. Makkouk, G.J. Weiner, Cancer immunotherapy and breaking immune tolerance: new approaches to an old challenge, Cancer Res 75(1) (2015) 5-10.

[38] J.B. Mitchem, D.J. Brennan, B.L. Knolhoff, B.A. Belt, Y. Zhu, D.E. Sanford, L. Belaygorod, D. Carpenter, L. Collins, D. Piwnica-Worms, S. Hewitt, G.M. Udupi, W.M. Gallagher, C. Wegner, B.L. West, A. Wang-Gillam, P. Goedegebuure, D.C. Linehan, D.G. DeNardo, Targeting tumor-infiltrating macrophages decreases tumor-initiating cells, relieves immunosuppression, and improves chemotherapeutic responses, Cancer Res 73(3) (2013) 1128-41.

[39] X.D. Liu, A. Hoang, L. Zhou, S. Kalra, A. Yetil, M. Sun, Z. Ding, X. Zhang, S. Bai, P. German, P. Tamboli, P. Rao, J.A. Karam, C. Wood, S. Matin, A. Zurita, A. Bex, A.W. Griffioen, J. Gao, P. Sharma, N. Tannir, K. Sircar, E. Jonasch, Resistance to Antiangiogenic Therapy Is Associated with an Immunosuppressive Tumor Microenvironment in Metastatic Renal Cell Carcinoma, Cancer Immunol Res 3(9) (2015) 1017-29.

[40] J. Tommelein, E. De Vlieghere, L. Verset, E. Melsens, J. Leenders, B. Descamps, A. Debucquoy, C. Vanhove, P. Pauwels, C.P. Gespach, A. Vral, A. De Boeck, K. Haustermans, P. de Tullio, W. Ceelen, P. Demetter, T. Boterberg, M. Bracke, O. De Wever, Radiotherapy-activated cancer-associated fibroblasts promote tumor progression through paracrine IGF-1R activation, Cancer Res 78(3) (2017) 659-670.

[41] S. Demaria, N. Kawashima, A.M. Yang, M.L. Devitt, J.S. Babb, J.P. Allison, S.C. Formenti, Immune-Mediated Inhibition of Metastases after Treatment with Local Radiation and CTLA-4 Blockade in a Mouse Model of Breast Cancer, Clin Cancer Res 11(2) (2005) 728-734.

[42] X. Wang, J.E. Schoenhals, A. Li, D.R. Valdecanas, H. Ye, F. Zang, C. Tang, M. Tang, C.G. Liu, X. Liu, S. Krishnan, J.P. Allison, P. Sharma, P. Hwu, R. Komaki, W.W. Overwijk, D.R. Gomez, J.Y. Chang, S.M. Hahn, M.A. Cortez, J.W. Welsh, Suppression of Type I IFN Signaling in Tumors Mediates Resistance to Anti-PD-1 Treatment That Can Be Overcome by Radiotherapy, Cancer Res 77(4) (2017) 839-850.

[43] A. Oweida, M.K. Hararah, A. Phan, D. Binder, S. Bhatia, S. Lennon, S. Bukkapatnam, B. Van Court, N. Uyanga, L. Darragh, H.M. Kim, D. Raben, A.C. Tan, L. Heasley, E. Clambey, R. Nemenoff, S.D. Karam, Resistance to Radiotherapy and PD-L1 Blockade Is Mediated by TIM-3 Upregulation and Regulatory T-Cell Infiltration, Clin Cancer Res 24(21) (2018) 5368-5380.

[44] M. Crittenden, H. Kohrt, R. Levy, J. Jones, K. Camphausen, A. Dicker, S. Demaria, S. Formenti, Current clinical trials testing combinations of immunotherapy and radiation, Semin Radiat Oncol 25(1) (2015) 54-64.

[45] S. Tran, P.J. DeGiovanni, B. Piel, P. Rai, Cancer nanomedicine: a review of recent success in drug delivery, Clin Transl Med 6(1) (2017) 44.

[46] S. Sindhwani, A.M. Syed, J. Ngai, B.R. Kingston, L. Maiorino, J. Rothschild, P. MacMillan, Y. Zhang, N.U. Rajesh, T. Hoang, J.L.Y. Wu, S. Wilhelm, A. Zilman, S. Gadde, A. Sulaiman, B. Ouyang, Z. Lin, L. Wang, M. Egeblad, W.C.W. Chan, The entry of nanoparticles into solid tumours, Nat Mater 19 (2020) 566–575.

[47] A.H. Bannister, K. Bromma, W. Sung, M. Monica, L. Cicon, P. Howard, R.L. Chow, J. Schuemann, D.B. Chithrani, Modulation of nanoparticle uptake, intracellular distribution, and retention with docetaxel to enhance radiotherapy, Br J Radiol 93(1106) (2020) 20190742.

[48] K.M. Au, Y. Min, X. Tian, L. Zhang, V. Perello, J.M. Caster, A.Z. Wang, Improving Cancer Chemoradiotherapy Treatment by Dual Controlled Release of Wortmannin and Docetaxel in Polymeric Nanoparticles, ACS Nano 9(9) (2015) 8976-96.

[49] B. Sun, C.T.t. Hagan, J. Caster, A.Z. Wang, Nanotechnology in Radiation Oncology, Hematol Oncol Clin North Am 33(6) (2019) 1071-1093.

[50] A.B. Satterlee, J.D. Rojas, P.A. Dayton, L. Huang, Enhancing Nanoparticle Accumulation and Retention in Desmoplastic Tumors via Vascular Disruption for Internal Radiation Therapy, Theranostics 7(2) (2017) 253-269.

[51] X. Tian, M. Nguyen, H.P. Foote, J.M. Caster, K.C. Roche, C.G. Peters, P. Wu, L. Jayaraman, E.G. Garmey, J.E. Tepper, S. Eliasof, A.Z. Wang, CRLX101, a Nanoparticle-Drug Conjugate Containing Camptothecin, Improves Rectal Cancer Chemoradiotherapy by Inhibiting DNA Repair and HIF1alpha, Cancer Res 77(1) (2017) 112-122.

[52] M.J. Neufeld, A.N. DuRoss, M.R. Landry, H. Winter, A.M. Goforth, C. Sun, Co-delivery of PARP and PI3K inhibitors by nanoscale metal–organic frameworks for enhanced tumor chemoradiation, Nano Res 12(12) (2019) 3003-3017.

[53] A. Mizrachi, Y. Shamay, J. Shah, S. Brook, J. Soong, V.K. Rajasekhar, J.L. Humm, J.H. Healey, S.N. Powell, J. Baselga, D.A. Heller, A. Haimovitz-Friedman, M. Scaltriti, Tumour-specific PI3K inhibition via nanoparticle-targeted delivery in head and neck squamous cell carcinoma, Nat Commun 8 (2017) 14292.

[54] Y. Zhang, F. Huang, C. Ren, J. Liu, L. Yang, S. Chen, J. Chang, C. Yang, W. Wang, C. Zhang, Q. Liu, X.J. Liang, J. Liu, Enhanced Radiosensitization by Gold Nanoparticles with Acid-Triggered Aggregation in Cancer Radiotherapy, Adv Sci 6(8) (2019) 1801806.

[55] S. Her, D.A. Jaffray, C. Allen, Gold nanoparticles for applications in cancer radiotherapy: Mechanisms and recent advancements, Adv Drug Deliv Rev 109 (2017) 84-101.

[56] Q. Chen, J. Chen, Z. Yang, J. Xu, L. Xu, C. Liang, X. Han, Z. Liu, Nanoparticle-Enhanced Radiotherapy to Trigger Robust Cancer Immunotherapy, Adv Mater 31(10) (2019) e1802228.

[57] S. Gao, T. Li, Y. Guo, C. Sun, B. Xianyu, H. Xu, Selenium-Containing Nanoparticles Combine the NK Cells Mediated Immunotherapy with Radiotherapy and Chemotherapy, Adv Mater 32(12) (2020) e1907568.

[58] K.M. Au, A. Tripathy, C.P. Lin, K. Wagner, S. Hong, A.Z. Wang, S.I. Park, Bespoke Pretargeted Nanoradioimmunotherapy for the Treatment of Non-Hodgkin Lymphoma, ACS Nano 12(2) (2018) 1544-1563.

[59] Y. Wen, X. Chen, X. Zhu, Y. Gong, G. Yuan, X. Qin, J. Liu, Photothermal-Chemotherapy Integrated Nanoparticles with Tumor Microenvironment Response Enhanced the Induction of Immunogenic Cell Death for Colorectal Cancer Efficient Treatment, ACS Appl Mater Interfaces 11(46) (2019) 43393-43408.

[60] W. Sun, Y. Du, X. Liang, C. Yu, J. Fang, W. Lu, X. Guo, J. Tian, Y. Jin, J. Zheng, Synergistic triple-combination therapy with hyaluronic acid-shelled PPy/CPT nanoparticles results in tumor regression and prevents tumor recurrence and metastasis in 4T1 breast cancer, Biomaterials 217 (2019) 119264.

[61] X. Song, Y. Krelin, T. Dvorkin, O. Bjorkdahl, S. Segal, C.A. Dinarello, E. Voronov, R.N. Apte, CD11b+/Gr-1+ immature myeloid cells mediate suppression of T cells in mice bearing tumors of IL-1beta-secreting cells, J Immunol 175(12) (2005) 8200-8.

[62] L. Cheng, J. Wang, X. Li, Q. Xing, P. Du, L. Su, S. Wang, Interleukin-6 induces Gr-1+CD11b+ myeloid cells to suppress CD8+ T cell-mediated liver injury in mice, PLoS One 6(3) (2011) e17631.

[63] D. Gabrilovich, T. Ishida, T. Oyama, S. Ran, V. Kravtsov, S. Nadaf, D.P. Carbone, Vascular endothelial growth factor inhibits the development of dendritic cells and dramatically affects the differentiation of multiple hematopoietic lineages in vivo, Blood 92(11) (1998) 4150-66.

[64] S.B. Coffelt, K. Kersten, C.W. Doornebal, J. Weiden, K. Vrijland, C.S. Hau, N.J.M. Verstegen, M. Ciampricotti, L. Hawinkels, J. Jonkers, K.E. de Visser, IL-17-producing gammadelta T cells and neutrophils conspire to promote breast cancer metastasis, Nature 522(7556) (2015) 345-348.

[65] Z. Granot, E. Henke, E.A. Comen, T.A. King, L. Norton, R. Benezra, Tumor entrained neutrophils inhibit seeding in the premetastatic lung, Cancer cell 20(3) (2011) 300-14.

[66] T. Takeshima, L.M. Pop, A. Laine, P. Iyengar, E.S. Vitetta, R. Hannan, Key role for neutrophils in radiation-induced antitumor immune responses: Potentiation with G-CSF, Proc Natl Acad Sci U S A 113(40) (2016) 11300-11305.

[67] K.T. Venmar, K.J. Carter, D.G. Hwang, E.A. Dozier, B. Fingleton, IL4 receptor ILR4α regulates metastatic colonization by mammary tumors through multiple signaling pathways, Cancer Res 74(16) (2014) 4329-40.

[68] M. Gaggianesi, A. Turdo, A. Chinnici, E. Lipari, T. Apuzzo, A. Benfante, I. Sperduti, S. Di Franco, S. Meraviglia, E. Lo Presti, F. Dieli, V. Caputo, G. Militello, S. Vieni, G. Stassi, M. Todaro, IL4 Primes the Dynamics of Breast Cancer Progression via DUSP4 Inhibition, Cancer Res 77(12) (2017) 3268-3279.

[69] Q. Chang, E. Bournazou, P. Sansone, M. Berishaj, S.P. Gao, L. Daly, J. Wels, T. Theilen, S. Granitto, X. Zhang, J. Cotari, M.L. Alpaugh, E. de Stanchina, K. Manova, M. Li, M. Bonafe, C. Ceccarelli, M. Taffurelli, D. Santini, G. Altan-Bonnet, R. Kaplan, L. Norton, N. Nishimoto, D. Huszar, D. Lyden, J. Bromberg, The IL-6/JAK/Stat3 feed-forward loop drives tumorigenesis and metastasis, Neoplasia 15(7) (2013) 848-62.

[70] C.O. Abana, B.S. Bingham, J.H. Cho, A.J. Graves, T. Koyama, R.T. Pilarski, A.B. Chakravarthy, F. Xia, IL-6 variant is associated with metastasis in breast cancer patients, PLoS One 12(7) (2017) e0181725.

[71] S. Zhao, D. Wu, P. Wu, Z. Wang, J. Huang, Serum IL-10 Predicts Worse Outcome in Cancer Patients: A Meta-Analysis, PLoS One 10(10) (2015) e0139598.

[72] P. Dentelli, A. Rosso, C. Olgasi, G. Camussi, M.F. Brizzi, IL-3 is a novel target to interfere with tumor vasculature, Oncogene 30 (2011) 4930.

[73] J. Zhang, A. Lu, D. Beech, B. Jiang, Y. Lu, Suppression of breast cancer metastasis through the inhibition of VEGF-mediated tumor angiogenesis, Cancer Ther 5 (2007) 273-286.

[74] S. Sasaki, T. Baba, T. Nishimura, Y. Hayakawa, S. Hashimoto, N. Gotoh, N. Mukaida, Essential roles of the interaction between cancer cell-derived chemokine, CCL4, and intra-bone CCR5-expressing fibroblasts in breast cancer bone metastasis, Cancer Lett 378(1) (2016) 23-32.

[75] L. Apetoh, F. Ghiringhelli, A. Tesniere, M. Obeid, C. Ortiz, A. Criollo, G. Mignot, M.C. Maiuri, E. Ullrich, P. Saulnier, H. Yang, S. Amigorena, B. Ryffel, F.J. Barrat, P. Saftig, F. Levi, R. Lidereau, C. Nogues, J.P. Mira, A. Chompret, V. Joulin, F. Clavel-Chapelon, J. Bourhis, F. Andre, S. Delaloge, T. Tursz, G. Kroemer, L. Zitvogel, Toll-like receptor 4-dependent contribution of the immune system to anticancer chemotherapy and radiotherapy, Nat Med 13(9) (2007) 1050-9.

[76] C. Villiers, M. Chevallet, H. Diemer, R. Couderc, H. Freitas, A. Van Dorsselaer, P.N. Marche, T. Rabilloud, From secretome analysis to immunology: chitosan induces major alterations in the activation of dendritic cells via a TLR4-dependent mechanism, Mol Cell Proteomics 8(6) (2009) 1252-64.

[77] T. Hamasaki, T. Uto, T. Akagi, M. Akashi, M. Baba, Modulation of gene expression related to Toll-like receptor signaling in dendritic cells by poly(gamma-glutamic acid) nanoparticles, Clin Vaccine Immunol 17(5) (2010) 748-56.

[78] T. Uto, T. Akagi, K. Yoshinaga, M. Toyama, M. Akashi, M. Baba, The induction of innate and adaptive immunity by biodegradable poly(gamma-glutamic acid) nanoparticles via a TLR4 and MyD88 signaling pathway, Biomaterials 32(22) (2011) 5206-12.

[79] R.B. Patel, M. Ye, P.M. Carlson, A. Jaquish, L. Zangl, B. Ma, Y. Wang, I. Arthur, R. Xie, R.J. Brown, X. Wang, R. Sriramaneni, K. Kim, S. Gong, Z.S. Morris, Development of an In Situ Cancer Vaccine via Combinational Radiation and Bacterial-Membrane-Coated Nanoparticles, Adv Mater 31(43) (2019) e1902626.

[80] C.L. Bueter, C.K. Lee, V.A. Rathinam, G.J. Healy, C.H. Taron, C.A. Specht, S.M. Levitz, Chitosan but not chitin activates the inflammasome by a mechanism dependent upon phagocytosis, J Biol Chem 286(41) (2011) 35447-55.

[81] S.F. Peng, M.T. Tseng, Y.C. Ho, M.C. Wei, Z.X. Liao, H.W. Sung, Mechanisms of cellular uptake and intracellular trafficking with chitosan/DNA/poly(gamma-glutamic acid) complexes as a gene delivery vector, Biomaterials 32(1) (2011) 239-48.

[82] S.D. Conner, S.L. Schmid, Regulated portals of entry into the cell, Nature 422(6927) (2003) 37-44.

[83] E.C. Carroll, L. Jin, A. Mori, N. Munoz-Wolf, E. Oleszycka, H.B.T. Moran, S. Mansouri, C.P. McEntee, E. Lambe, E.M. Agger, P. Andersen, C. Cunningham, P. Hertzog, K.A. Fitzgerald, A.G. Bowie, E.C. Lavelle, The Vaccine Adjuvant Chitosan Promotes Cellular Immunity via DNA Sensor cGAS-STING-Dependent Induction of Type I Interferons, Immunity 44(3) (2016) 597-608.

[84] Y.M. Vasiliev, Chitosan-based vaccine adjuvants: incomplete characterization complicates preclinical and clinical evaluation, Expert Rev Vaccines 14(1) (2015) 37-53.

[85] F. Furlani, P. Sacco, E. Decleva, R. Menegazzi, I. Donati, S. Paoletti, E. Marsich, Chitosan Acetylation Degree Influences the Physical Properties of Polysaccharide Nanoparticles: Implication for the Innate Immune Cells Response, ACS Appl Mater Interfaces 11(10) (2019) 9794-9803.

[86] D.P. Vasconcelos, A.C. Fonseca, M. Costa, I.F. Amaral, M.A. Barbosa, A.P. Aguas, J.N. Barbosa, Macrophage polarization following chitosan implantation, Biomaterials 34(38) (2013) 9952-9.

[87] W. Lee, S.H. Lee, D.G. Ahn, H. Cho, M.H. Sung, S.H. Han, J.W. Oh, The antiviral activity of poly-gamma-glutamic acid, a polypeptide secreted by Bacillus sp., through induction of CD14-dependent type I interferon responses, Biomaterials 34(37) (2013) 9700-8.

[88] Y. Ghendon, S. Markushin, Y. Vasiliev, I. Akopova, I. Koptiaeva, G. Krivtsov, O. Borisova, N. Ahmatova, E. Kurbatova, S. Mazurina, V. Gervazieva, Evaluation of properties of chitosan as an adjuvant for inactivated influenza vaccines administered parenterally, J Med Virol 81(3) (2009) 494-506.

[89] N.A.H. Dzung, N. T. N.; Van, D. T. H.; Phuong, N. T. L.; Quynh, N. T. N.; Hiep, D. M.; Hiep L. V., Chitosan Nanoparticle as a Novel Delivery System for A/H1n1 Influenza Vaccine: Safe Property and Immunogenicity in Mice, World Acad Sci Eng Technol 5(12) (2011) 5089.

[90] T.M. Jelacic, W.J. Ribot, J. Chua, A.E. Boyer, A.R. Woolfitt, J.R. Barr, A.M. Friedlander, Human Innate Immune Cells Respond Differentially to Poly-gamma-Glutamic Acid Polymers from Bacillus anthracis and Nonpathogenic Bacillus Species, J Immunol 204(5) (2020) 1263-1273.

[91] C. Marques, C. Som, M. Schmutz, O. Borges, G. Borchard, How the Lack of Chitosan Characterization Precludes Implementation of the Safe-by-Design Concept, Front Bioeng Biotechnol 8 (2020) 165.

Supplementary Methods:

Transmission electron microscopy of Ch/γ-PGA NPs

Briefly, a drop of the Ch/γ-PGA NPs suspension was placed onto a 400-mesh copper grid. After 2 min of deposition, the grid was tapped with a filter paper. TEM micrographs were obtained using a Jeol JEM 1400 electron microscope.

Fourier Transform Infrared Spectroscopy of Ch/γ-PGA NPs

The Ch/γ-PGA NPs were analyzed by FTIR-ATR spectroscopy, on a FTIR system 2000, PerkinElmer, Massachusetts, USA. The samples were scanned 32x from 400 to 4,000 cm^{-1} with 4 cm^{-1} resolution.

Supplementary Figures:

Supplementary Figure S1

A

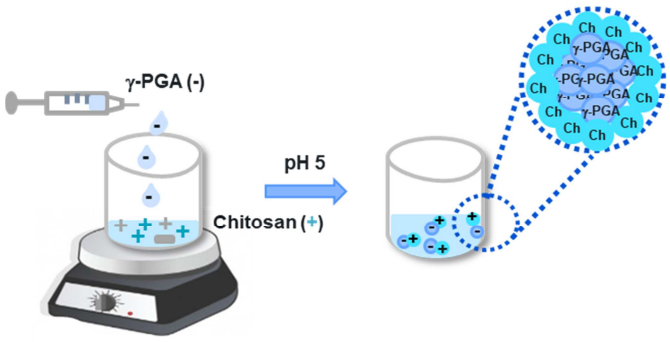

B

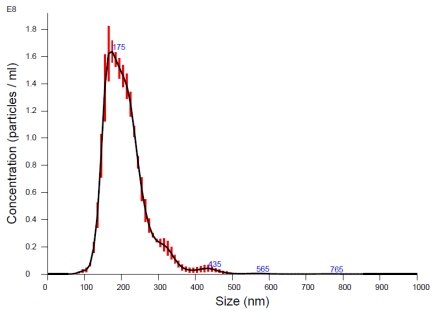

C

	Particle size (nm)	Polydispersity index	Zeta potential (mV)	Concentration (particles/mL)
Ch/γ-PGA NPs	210.8 ± 1.4	0.2 ± 0.05	18.7 ± 0.9	$1.87x10^{12}$ ± $9.83x10^{7}$

D

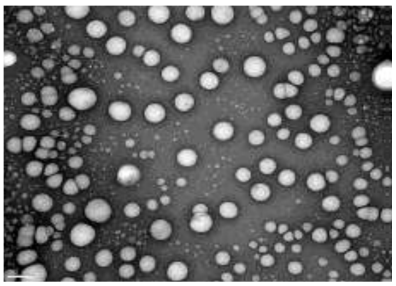

E

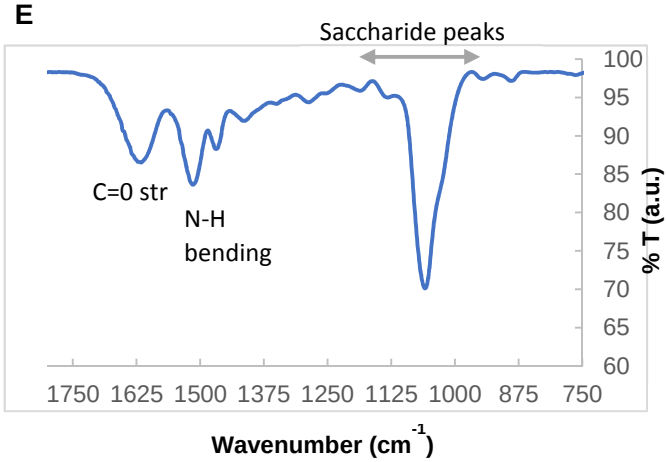

Figure S1. Ch/γ-PGA nanoparticles characterization. A. Schematic representation of Ch/γ-PGA nanoparticles (NPs) preparation. NPs were obtained by complex co-acervation method, driven by electrostatic interactions between chitosan and poly(γ-glutamic acid) (γ-PGA) at pH 5. γ-PGA solution was dropped to Ch solution under high stirring at room temperature, as previously described. Ch/γ-PGA NPs morphology was evaluated using a Jeol JEM 1400 transmission electron microscope (TEM). Samples were prepared by placing a drop of the NPs suspension onto a 400 µm mesh copper grid coated with carbon. After 2 min of deposition, TEM images were acquired with a magnification of 50,000x. Scale bar: 0,2µm. **B and C.** Nanoparticles size (nm), polydispersion index, zeta potential (mV) were evaluated by dynamic light (DLS) scattering and the concentration (particles/mL) through NTA 3.3 Dev Build 3.3.104. **D**. Ch/γ-PGA NPs morphology was evaluated using a Jeol JEM 1400 transmission electron microscope (TEM). Samples were prepared by placing a drop of the NPs suspension onto a 400 µm mesh copper grid coated with carbon. After 2 min of deposition, TEM images were acquired with a magnification of 50,000x. Scale bar: 0,2µm. **E.** FTIR spectra of Ch/γ-PGA NPs.

Supplementary Figure S2

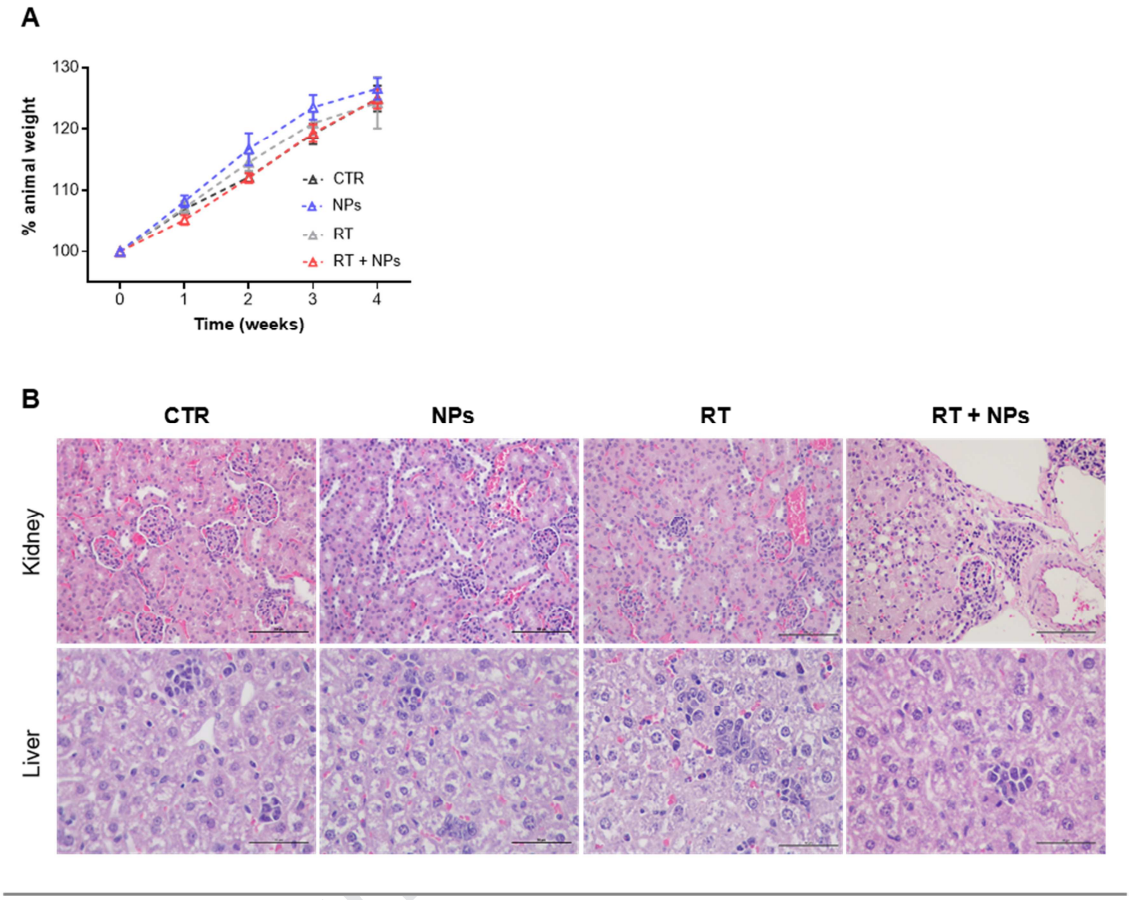

Figure S2. The distinct treatments do not impact animal weight, neither liver nor kidney histology. **A.** Animal body weight was evaluated every week during 4 weeks. Time 0 corresponds to the week before tumor cells inoculation. **B.** Mice liver and kidney were processed for histological procedures and stained with hematoxylin and eosin. Kidney images: magnification 200x; scale bar: 100 µm. Liver images: magnification 400x; scale bar: 50 µm. Data show the mean ± SEM and it is representative of at least 7 animals. All comparisons were performed using the Kruskal Wallis test followed by Dunn's multiple comparison test relative to non-treated control or single treatments (NPs or RT). No significant differences were found.

Supplementary Figure S3

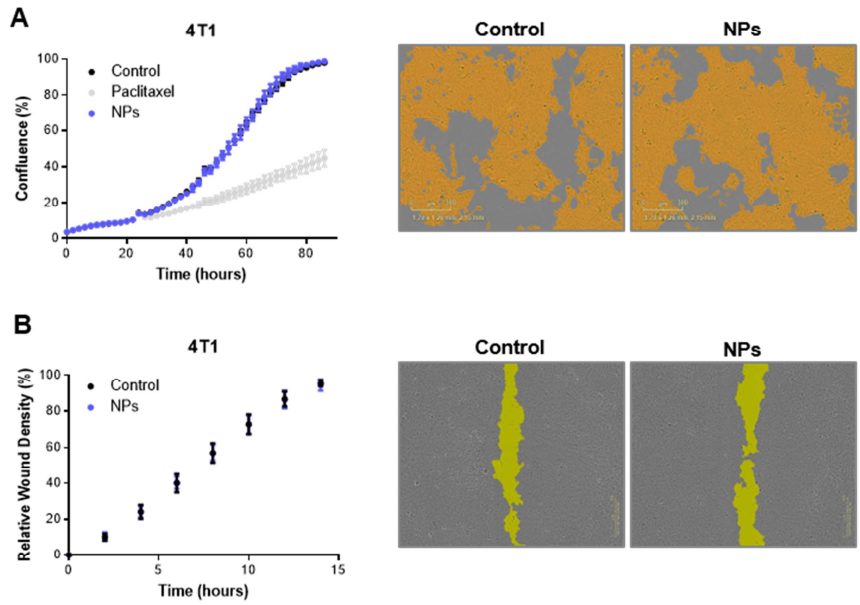

Figure S3 –Ch/γ-PGA nanoparticles did not impact the 4T1 cell line proliferation nor migration. 4T1-Luc cells were stimulated with 0.7 mg/mL of Ch/γ-PGA nanoparticles, with 5 nM paclitaxel (positive control) or left without treatment. **A.** Real-time analysis of cell confluency of treated 4T1-Luc cells using IncuCyte technology. Microscopic pictures were taken every 2 h and confluency was determined using IncuCyte software (indicated by yellow mask, right panel). **B.** Relative wound density was analyzed using IncuCyte software (scratch wound is indicated by yellow mask, right panel). In **A and B** a representative example of three biological replicates is presented. Mean ± SD of six technical replicates is shown.

Supplementary Figure S4

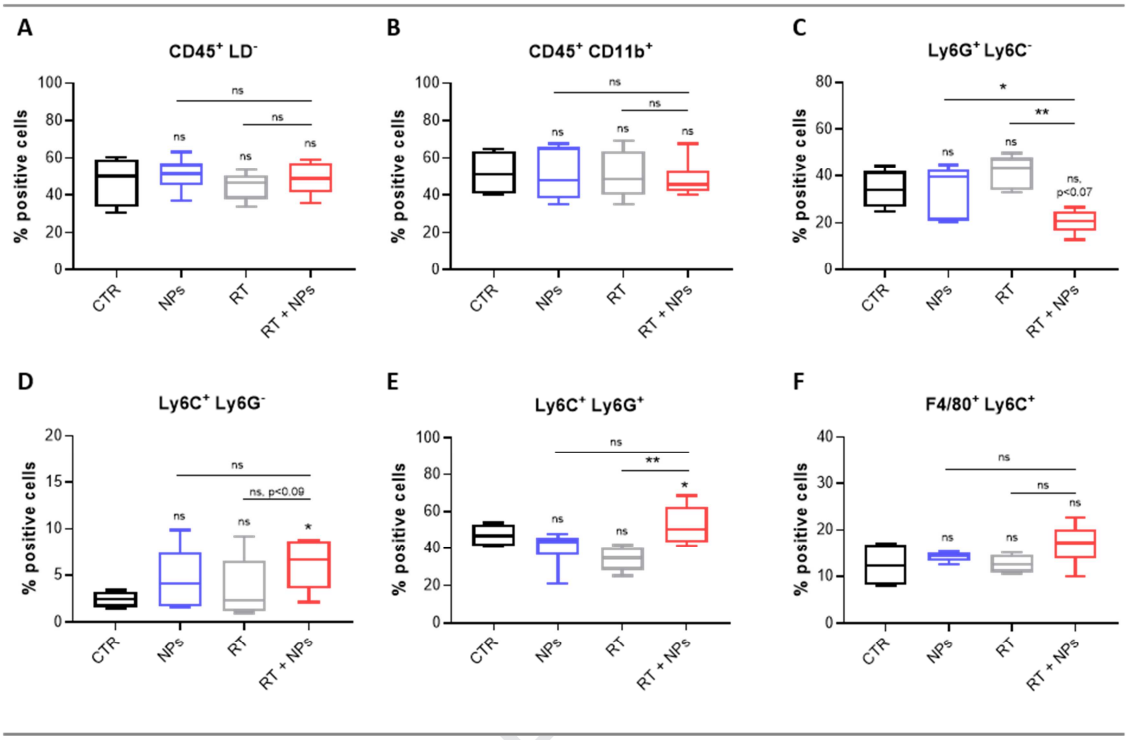

Figure S4 – **Radiotherapy in combination with Ch/γ-PGA nanoparticles decreases the accumulation of granulocytic-myeloid derived suppressor cells and increases the accumulation of neutrophils and monocytic-myeloid derived suppressor cells at the primary tumor site.** Mice injected with 4T1-Luc cells on the mammary fat pad were treated with radiotherapy (RT) (2x5 Gy), with Ch/γ-PGA NPs (NPs) or with RT combined with Ch/γ-PGA NPs (RT+NPs). Non-treated animals were used as control (CTR). Tumors were collected and processed for flow cytometry analysis. The pseudocolor plots indicating the myeloid cells gate strategy is showed in Fig. 3A. $CD45^+$Live Dead $(LD)^-$ cells were gated on single cells (FSC-A vs SSC-H). $CD11b^+$ cells were gated on $CD45^+LD^-$ cells. $Ly6C^+Ly6G^-$, $Ly6C^-Ly6G^+$, $Ly6C^+Ly6G^+$, $F4/80^+Ly6C^+$ cells were gated on $CD11b^+$ cells. **A-F.** The percentage of positive cells was determined. Data is representative of at least 5 animals per group. Median is represented by the horizontal line inside the box plots. All comparisons were performed using the Kruskal Wallis test followed by Dunn's multiple comparison test (*p<0.05 and **p<0.01 relative to non-treated CTR or single treatments (NPs or RT)). p≤0.1 were represented in the graphs.

Supplementary Figure S5

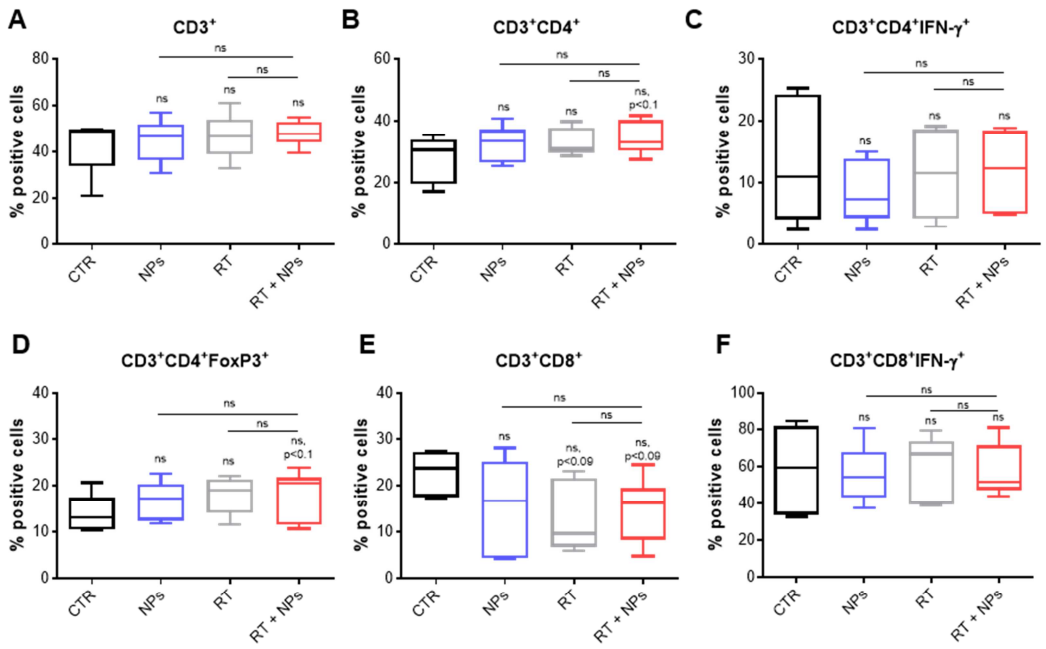

Figure S5 – Radiotherapy in combination with Ch/γ-PGA nanoparticles does not significantly impact the accumulation of T cells at the primary tumor site. Mice injected with 4T1-Luc cells on the mammary fat pad were treated with radiotherapy (RT) (2x5 Gy), with Ch/γ-PGA NPs (NPs) or with RT combined with Ch/γ-PGA NPs (RT+NPs). Non-treated animals were used as control (CTR). Tumors were collected and processed for flow cytometry analysis. The T cells gate strategy was similar to the applied in the spleen analysis, Fig. 4A. $CD45^+$Live Dead $(LD)^-$ cells were gated on single cells (FSC-A vs SSC-H). $CD3^+$, $CD3^+CD4^+$, $CD3^+CD8^+$ T cells were gated on $CD45^+LD^-$ cells. IFN-γ-producing T cells were gated on $CD3^+CD4^+$ or $CD3^+CD8^+$ T cells. FoxP3-expressing cells were gated on $CD3^+CD4^+$ T cells. **A-F.** The percentage of positive cells was determined. Data is representative of at least 5 animals per group. Median is represented by the horizontal line inside the box plots. All comparisons were performed using the Kruskal Wallis test followed by Dunn's multiple comparison test. p≤0.1 were represented in the graphs.

Supplementary Figure S6

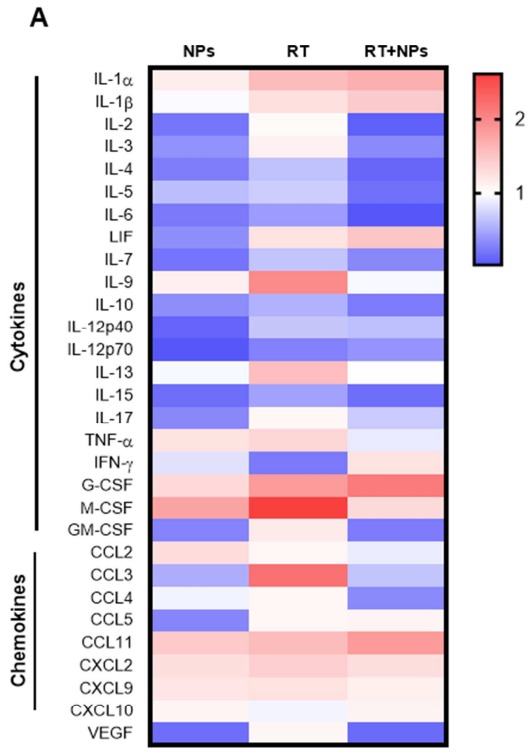

Figure S6 – **Radiotherapy in combination with Ch/γ-PGA nanoparticles modulates the systemic immune profile.** Mice were subcutaneously injected with 4T1-Luc cells were treated with radiotherapy (RT) (2x5 Gy), with Ch/γ-PGA NPs (NPs) or with RT combined with Ch/γ-PGA NPs (RT+NPs). Non-treated animals were used as control (CTR). At day 28, animals were euthanized, and serum was collected for analysis through Multiplex immunobead assay technology. Outliers were calculated through ROUT method (Q=1%) and removed from the analysis. **A.** Heatmap of cytokines, chemokines, and growth factors (VEGF) in serum from at least 5 animals per group. Soluble factors concentration from treated-animals was compared to the concentration values of non-treated animals (CTR). Fold changes are presented as heatmap. Red, white, and blue indicate induction, no change, and inhibition, respectively.

Author Contributions

FC was responsible for conceptualization, methodology, investigation, formal analysis, and writing of original draft ; MLP was involved in conceptualization, formal analysis, and writing - review & editing; CLP and FG was participated in the methodology and writing - review & editing; KS, MAB and KV provided resources and writing - review & editing; RMG and OdW were involved in the supervision, providing resources, and writing - review & editing and MJO was responsible for conceptualization, supervision, funding acquisition, project administration and writing - review & editing.